

DISORDER INDUCED ELECTRONIC AND MAGNETIC PROPERTIES OF GRAPHENE QUANTUM DOTS

**A Thesis Submitted to
the Graduate School of Engineering and Sciences of
İzmir Institute of Technology
in Partial Fulfillment of the Requirements for the Degree of**

MASTER OF SCIENCE

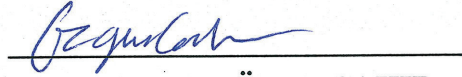
in Physics

**by
Erdoğan Bulut KUL**

**July 2019
İZMİR**

We approve the thesis of **Erdoğan Bulut KUL**

Examining Committee Members:



Assoc. Prof. Dr. Özgür ÇAKIR
Department of Physics, İzmir Institute of Technology



Assoc. Prof. Dr. A. Devrim GÜÇLÜ
Department of Physics, İzmir Institute of Technology

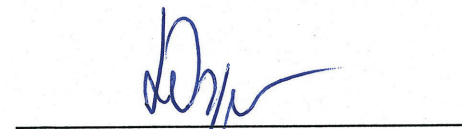


Prof. Dr. Serpil ŞAKİROĞLU
Department of Physics, Dokuz Eylül University


11 July 2019



Assoc. Prof. Dr. A. Devrim GÜÇLÜ
Supervisor, Department of Physics
İzmir Institute of Technology



Prof. Dr. Lütfi ÖZYÜZER
Head of the Department of
Physics



Prof. Dr. Aysun SOFUOĞLU
Dean of the Graduate School of
Engineering and Sciences

ACKNOWLEDGMENTS

I would like to thank my supervisor Assoc. Prof. Dr. A. Devrim Güçlü. Taking lessons from his way of working, helped me to improve my studying behaviour in a scientific manner. His patience gave me the encouragement to making mistakes and his support helped me to learn from them. Also I never felt rushed to do something, I've always find time to enjoy what I'm doing.

I am also thankful to the committee members of my thesis Assoc. Prof. Dr. Özgür Çakır and Prof. Dr. Serpil Şakirođlu for their participations and proofreading.

My group mates Anıl Kolay and Mustafa Polat always came with the good questions and made me think and when I had a question they used all their skills to make me understand and if they weren't know the answer they made thought experiments with me.

Thanks to my friends Gökhan Öztarhan, A. Utku Canbolat, Elif Ünsal, Sinem Duman and Emre Okcu, I never felt depressed in hard situations. They are the people who love making science and living like me. So, I've always learned something even we are chattering.

I am also thankful to my family. Nothing I would write here enough to describe their importance to me.

This work was supported by The Scientific and Technological Research Council of Turkey(TUBITAK) under the 1001 Grant Project No.116F152.

ABSTRACT

DISORDER INDUCED ELECTRONIC AND MAGNETIC PROPERTIES OF GRAPHENE QUANTUM DOTS

In this thesis, we aim to study magnetic properties of hexagonal shaped graphene quantum dots with armchair edge in the case of atomic collapse by modelling two vacancies on it. The measured relativistic electron transport property of the graphene allows us to observe the phenomenon called "atomic collapse" in a small energy scale which existence is proven theoretically before for atoms whose atomic number is higher than 170. First we modelled a Coulomb potential at the center of a hexagonal shaped and armchair edged GQD and examined by using tight-binding method. We obtain similar results with previous works. After that, we started to study magnetic properties of the dot by mean-field Hubbard method which includes spins into calculation. We modelled a vacancy close to the center of the dot and examined electronic and magnetic properties by MFH method. Also we modelled two vacancies on the dot that we changed the distance between them and the direction respectively. Also by applying Coulomb potential at the center of the vacancies we examined magnetic behaviour at the atomic collapse regime. Also, we compared our results with the works obtained by using RKKY (Ruderman-Kittel-Kasuya-Yosida) interaction method which considers the indirect interactions of magnetic impurities that uses electrons of metallic substrates. We found that increasing Coulomb potential and increasing distance between the vacancies, reduces correlations of electrons around the vacancies. The ground state energy difference between ferromagnetic and anti-ferromagnetic systems, that proportional to interaction strength, shows similar behaviour that has been observed by using RKKY method. Also if we take out two atoms from the same sublattice and with the same spin property, changing Coulomb potential leads to ferromagnetic-anti-ferromagnetic phase transition, independent from the atomic collapse behaviour. Also we observed that there is no direct link between the magnetic transition and the energy difference of the vacancy states.

ÖZET

GRAFEN KUANTUM NOKTALARIN DÜZENSİZLİKLERDEN DOĞAN ELEKTRİK VE MANYETİK ÖZELLİKLERİ

Bu tezde, armchair kenarlı, altıgen şeklindeki Grafen Kuantum Noktalarında iki boşluk modelleyerek, atomik çökme bölgesindeki manyetik davranışlarını incelemeyi hedefledik. Grafenin ölçülen, relativistik elektron iletim özelliği bizi; atom numarası 170'ten fazla olan atomlar için varlığı teorik olarak ispat edilmiş, atomik çökme davranışını düşük enerji seviyelerinde gözlemlememize izin verir. İlk olarak; grafende görülen atomik çökme durumunu, armchair kenarlı altıgen grafen Kuantum Noktalarında merkeze bir Coulomb potansiyeli koyup, sıkı bağ modelini kullanarak inceledik ve literatür ile uyumlu sonuçlar elde ettik. Bunun üzerine elektron spinlerini de hesaba katan bir model olan ortalama-alan Hubbard modelini kullanarak, kuantum noktanın manyetik özelliklerini incelemeye geçtik. Kullandığımız grafen kuantum noktaları üzerinde iki adet atomik boşluk modelleyip, aralarındaki mesafeyi ve duruş yönlerini değiştirdik. Ayrıca yarattığımız boşlukların bulunduğu pozisyonlara Coulomb potansiyeli uygulayarak atomik çökme bölgesindeki manyetik davranışları gözlemledik. Ayrıca, elde ettiğimiz sonuçlarla RKKY (Ruderman-Kittel-Kasuya-Yosida) etkileşimi modeline göre elde edilmiş sonuçları karşılaştırdık. Bu model manyetik momente sahip safsızlık atomlarının metale ait elektronlar vasıtasıyla dolaylı bir şekilde birbiriyle etkileşimini tanımlar. Yaptığımız çalışmalarda artan Coulomb potansiyelinin ve atomik boşluklar arasındaki artan mesafenin atomik boşluklar etrafındaki elektronlar arasındaki korelasyonu azalttığını gözlemledik. Ferromanyetik ve anti-ferromanyetik taban durumu enerji farkı ile orantılı olan; etkileşim katsayısının önceden RKKY metodu ile bulunan sonuçlarla uyumlu sonuç verdiğini bulduk. Ayrıca değişen Coulomb potansiyelinin atomik çökme davranışından bağımsız olarak ferromanyetik-anti-ferromanyetik faz değişimine yol açtığını gözlemeledik (AA durumu). Ayrıca manyetik faz değişimi ile atomik boşluk durumlarının enerji farkları arasında direkt bir bağlantı olmadığını gözlemledik.

TABLE OF CONTENTS

LIST OF FIGURES	vii
LIST OF ABBREVIATIONS	x
CHAPTER 1. INTRODUCTION	1
CHAPTER 2. THEORETICAL FOUNDATIONS	6
2.1. Tight-Binding Model.....	6
2.2. Mean-Field Hubbard Model	14
2.3. Further Calculation Details	19
CHAPTER 3. DISORDERS AND GRAPHENE	20
3.1. Absence of Backscattering.....	20
3.2. Long-Range Disorder	20
3.3. Short-Range Disorders	20
3.4. Supercritical Disorders.....	21
CHAPTER 4. DEFECT EFFECTS IN GQDS	25
4.1. Single Defect Effects.....	25
4.2. Magnetic Correlations Between Defects	32
CHAPTER 5. CONCLUSION	40
REFERENCES	41

LIST OF FIGURES

<u>Figure</u>	<u>Page</u>
Figure 1.1	Graphene(left) consists of a 2D hexagonal lattice of carbon atoms and Graphite(right) is a stack of graphene layers(Source: Neto et al. (2006)) 1
Figure 1.2	Comparison of graphene producing methods respect to their qualities and prices. (Source: Novoselov et al. (2012)). 2
Figure 1.3	Graphene with (a) zigzag edge and (b) armchair edge.(Source: Nikolai A. Poklonski (2012)) 3
Figure 1.4	Single-particle tight-binding spectrum of (a) armchair hexagonal, (b) zigzag hexagonal, and (c) zigzag triangular graphene quantum dot structures consisting of similar number of carbon atoms ($t=-2.8$ eV). Top panel shows the atomic positions.(Source: Sheng et al. (2012)) 4
Figure 1.5	Schematic drawing of the atomic bounding energies as function of the atomic number Z and the level diving process in the supercritical regime. The dotted curves indicate the solutions for a point charge while the solid curves take into account the finite size of the nucleus (Source: Moldovan and Peeters (2016)) 5
Figure 2.1	(a) Lattice structure of graphene. (b) sp^2 hybridization of carbon atoms to form the 2D crystal structure of graphene as well as delocalized π orbitals.(Source: Liang (2014)). 7
Figure 2.2	(a) Band structure of Graphene, (b) Closeup to Fermi Level. 11
Figure 2.3	Symmetry points of Graphene. 12
Figure 2.4	A benzene ring(Source: Guclu (2014)). 13
Figure 3.1	Evolution of charged impurity clusters from subcritical to supercritical regime. (A to E) dI/dV spectra measured at different distances from the center of Ca dimer clusters (i.e., artificial nuclei) composed of one to five dimers. (F to J) Theoretical normalized dI/dV spectra (obtained from the Dirac equation) for graphene at the same distances from dimer clusters as in (A) to (E). (Source: Wang et al. (2013)) 24
Figure 4.1	Visualization of applied potential with a cut-off area(red area) on hexagonal GQD with armchair edge. 25
Figure 4.2	TB eigenenergies vs beta for armchair edged hexagonal GQD(14622 Atoms) with $s_{nne}=0$ eV 26

Figure 4.3	Corresponding probability densities for specific beta values pointed in Fig. (4.2) versus $\rho = r/R$	27
Figure 4.4	(a) Energy spectrum for a dot with a Coulomb impurity. The dashed curves are for a point impurity and the solid ones for a finite size impurity of radius equal to the lattice parameter.(b) Probability density vs ρ for the points labeled by (1) to (4) in (a).(Source: Van Pottelberge et al. (2017))	28
Figure 4.5	(a) TB eigenenergies vs beta for armchair edged hexagonal GQD(5514 Atoms) with $s_{\text{ne}}=0$ eV and (b) $s_{\text{ne}}=-0.1$ eV.	28
Figure 4.6	(a),(b)Tight Binding and (c),(d) Mean-Field Hubbard results for armchair edged hexagonal GQD(5514 Atoms) with $s_{\text{ne}}=0$ eV and $s_{\text{ne}}=-0.1$	29
Figure 4.7	(a)Tight Binding results for hexagonal shaped GQD with armchair edge(5513 Atoms), $s_{\text{ne}}=0$ eV. Mean-Field Hubbard results (b) up electron and (c) down electron eigenenergies for the same configuration. Red lines stand for the vacancy states.	30
Figure 4.8	Spin densities for the single vacancy configuration with (a) beta=0.20, (b) beta=0.75, (c) beta=1.21, (d) beta=1.80.	31
Figure 4.9	Two toy models to show how the vacancies moving along in (a) zigzag and (b) armchair direction. The A site that pointed with the star sign indicates the fixed vacancy. The other vacancy moves on the other points.	32
Figure 4.10	Ground state energy difference $-(E_{S_z=1} - E_{S_z=0})$ in logarithmic scale (inset: real) for AA case on (a) zigzag and (b) armchair direction calculated by using MFH for hexagonal GQD with armchair edge with double vacancy(5512 Atoms). The red lines stands for $s_{\text{ne}}=0$ eV, the orange ones for $s_{\text{ne}}=-0.1$ and the black ones for $s_{\text{ne}}=-0.2$ eV.	33
Figure 4.11	Ground state energy difference $E_{S_z=1} - E_{S_z=0}$ in logarithmic scale(inset: real) for AB case on (a) zigzag and (b) armchair direction calculated by using MFH for hexagonal GQD with armchair edge with double vacancy(5512 Atoms). The dark blue lines stands for $s_{\text{ne}}=0$ eV, the light blue ones for $s_{\text{ne}}=-0.1$ and the black ones for $s_{\text{ne}}=-0.2$ eV.	34
Figure 4.12	Spin densities for the two vacancy AA configuration for distance(a) 0 atom, (b) 5 atoms, and(c) 10 atoms.	35
Figure 4.13	Ground state energy difference $E_{S_z=1} - E_{S_z=0}$ for AA case on zigzag	

direction for (a) snne=0 eV, (b) snne=-0.1 eV and armchair direction for (c) snne=0 eV, (d) snne=-0.1 eV calculated by using MFH for hexagonal GQD with armchair edge with double vacancy(5512 Atoms).	36
Figure 4.14 Ground state energy difference $E_{S_z=1} - E_{S_z=0}$ for AB case on zigzag direction for (a) snne=0 eV, (b) snne=-0.1 eV and armchair direction for (c) snne=0 eV, (d) snne=-0.1 eV calculated by using MFH for hexagonal GQD with armchair edge with double vacancy(5512 Atoms).	37
Figure 4.15 The first and second vacancy states and the the first three states above the fermi level on zigzag direction	38
Figure 4.16 AA case on zigzag direction. TB eigenenergy difference between the vacancy states for AA case with (a) snne=0 eV, (b) snne=-0.1 eV, and AB case with (c) snne=0 eV, (d) down spin energy matrix with snne=-0.1 eV	39

LIST OF ABBREVIATIONS

TB	Tight-Binding
GQD	Graphene Quantum Dot
MFH	Mean Field Hubbard
RKKY	Ruderman-Kittel-Kasuya-Yosida
snne	Second Nearest Neighbour Energy
FM	Ferromagnetic
AFM	Anti-Ferromagnetic



CHAPTER 1

INTRODUCTION

Graphene is a two-dimensional crystal structure with thickness of one atomic layer, made up from only carbon atoms(Novoselov et al. (2004)). Even though graphene was investigated many times since 1947, the work of P. R. Wallace(Wallace (1947)), it's popularity came after Geim and Novoselov's work on isolation of graphene by mechanical exfoliation which was awarded with Nobel prize in 2010(Novoselov et al. (2004)).

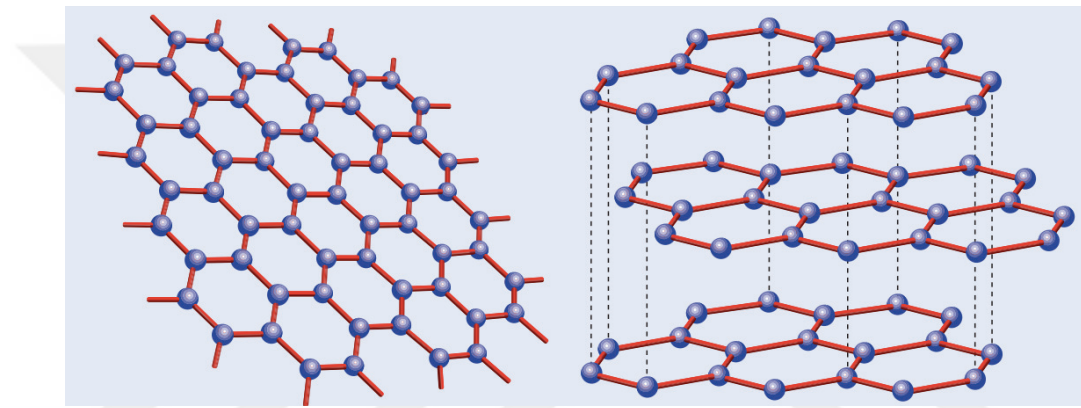


Figure 1.1. Graphene(left) consists of a 2D hexagonal lattice of carbon atoms and Graphite(right) is a stack of graphene layers(Source: Neto et al. (2006))

By treating one single layer of graphite by tight-binding method; Wallace found interesting results like, electrons' massless Dirac-fermion behaviour at this structure and that is a semimetal with zero energy band gap. Then Geim and Novoselov synthesised this theoretical matter by only using a scotch tape. This method's scientific name is "mechanical exfoliation", but it's known as "scotch tape method" because of Novoselov, Geim and co-workers used a scotch tape to obtain graphene in 2004(Novoselov et al. (2004)). Scotch tape's adhesivity overwhelms weak van der Waals forces, and that bonds between graphite's layers brake by mechanical force. So, peeling off repeatedly, single layer of graphite(graphene) can be obtained. Even though application of this method is easy and low costed, samples are obtained are too small to use(up to $10 \mu m$) for commercial purposes.

Many theoretical properties of graphene predicted after the Wallace's work and

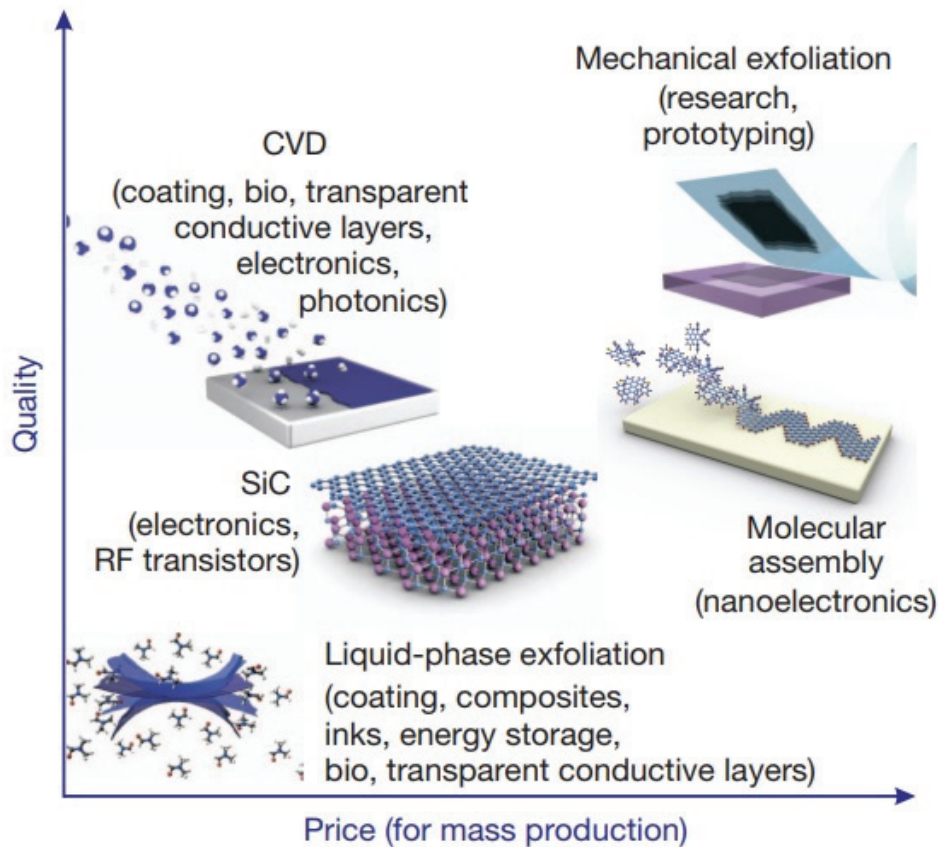


Figure 1.2. Comparison of graphene producing methods respect to their qualities and prices. (Source: Novoselov et al. (2012)).

there are new methods to obtain graphene(Juang et al. (2010); Reina et al. (2009); Berger et al. (2004); Boukhvalov and Katsnelson (2008); Staudenmaier (1898)).

One of them is CVD synthesis technique. This technique provides few or multilayer graphene films with high quality and large-scale(Juang et al. (2010)). There are different ways to obtain graphene in this method.(Juang et al. (2010); Reina et al. (2009)) Basically, the method involves carbon based gaseous precursor's disassociation at high temperatures in high vacuum. Then by cooling the chamber, a thin film of carbon atoms forms on a the substrate.

The other one is thermal Decomposition of SiC. The SiC crystal is heated at high temperatures between 1250 C° and 1450 C° for 1-20 min. Under these conditions Si sublimates, and the C atoms forms thin graphite layers(Berger et al. (2004)).

Other than this methods; Reduction of Graphite Oxide(GO) method, produce graphitic oxide, sometimes called graphitic acid by using intercalated graphite compounds.

There are several ways developed by Hummers(Hummers and Offeman (1958)), Brodie(Brodie (1859)), and Staudenmeier(Staudenmaier (1898)). Because of the hybridization type of carbon atoms changes sp^2 to sp^3 , final samples has energy gap in the electron density of states(Boukhalov and Katsnelson (2008)). But depending on hydrophilic character, GO is easy to disperse in water therefore it can be used intercalation compound in different materials(Stankovich et al. (2007)).

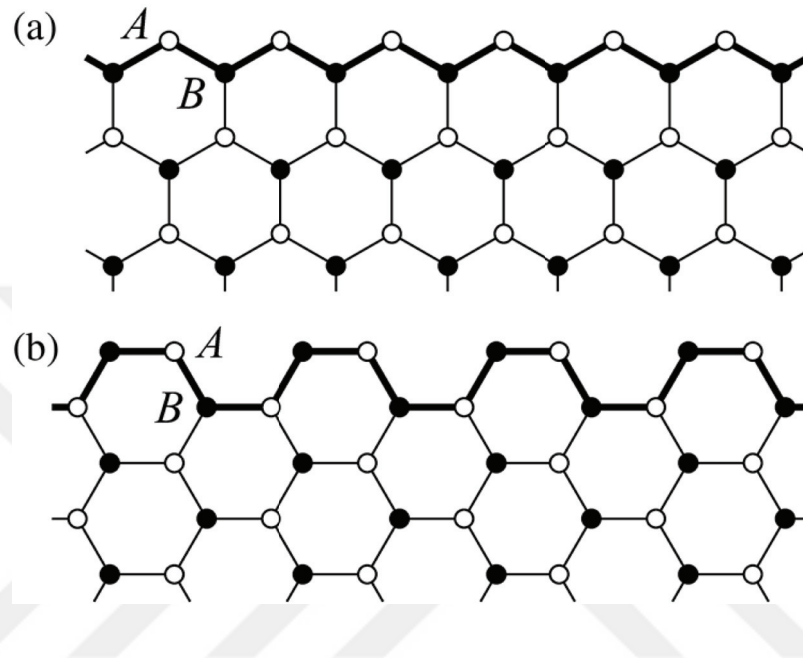


Figure 1.3. Graphene with (a) zigzag edge and (b) armchair edge.(Source: Nikolai A. Poklonski (2012))

Graphene can be fabricated in different size and shapes(nanoribbon, nanotube, quantum dot, fullerene etc.) in order to obtain some specific characteristics. One of them is GQD, which is the main material in this thesis. Sizes of GQDs can go up to 10 layers high and width of 100 nanometers(Li et al. (2013)). Fabrication of GQDs can be considered in two main title; the first one is top-down method which means the direct cutting of graphene-like materials (i.e. graphene oxide, graphene, carbon nanotubes, graphite powder and coal etc.) into dot size by using various processes. The second one is bottom-up method, which uses graphene-like smaller polycyclic aromatic hydrocarbons (PAHs) molecular precursors (such as fullerene, benzene, hexaperi-hexabenzocoronene, glucose etc.). Those are goes into chemical reactions to build GQDs up(Tian et al. (2018)).

GQDs can be found in different shapes(triangular, hexagonal, etc.) with different edge types(zigzag, armchair, mixed)(Fig. 1.3) and each combination has different bandgap properties(Guclu (2014)). In Fig. (1.4), we see how those edge types strongly

related to energy spectrum. For the hexagonal-shaped GQD with zigzag edge, there is a small band gap while hexagonal-shaped GQD with armchair edge and triangular-shaped GQD with zigzag edge have a well defined gap around $0.2t$. Also the triangular zigzag dot has degenerate energy levels at the Fermi level.

While creating those kind of dots in desired shapes, if free electrons on edges interact with the substrate it seriously affects the properties of graphene. In order to prevent this effect, passivation of dangling σ bonds is in use(Liu et al. (2017)).

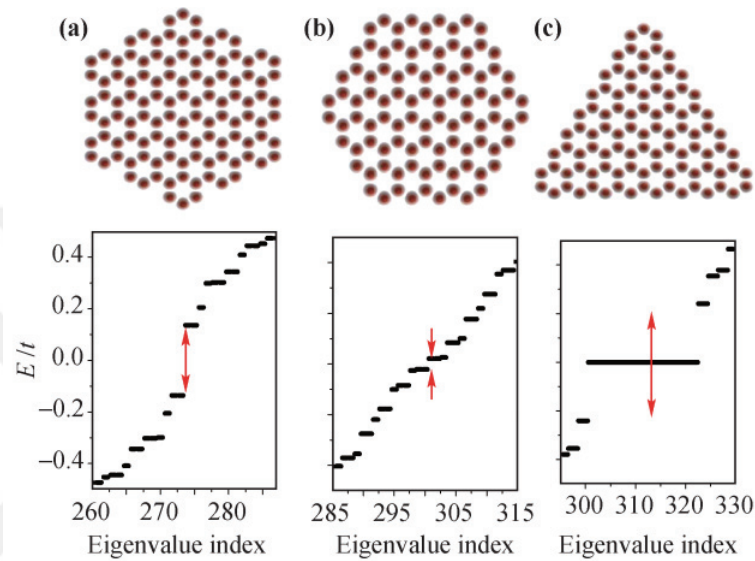


Figure 1.4. Single-particle tight-binding spectrum of (a) armchair hexagonal, (b) zigzag hexagonal, and (c) zigzag triangular graphene quantum dot structures consisting of similar number of carbon atoms ($t=-2.8$ eV). Top panel shows the atomic positions.(Source: Sheng et al. (2012))

One of the theoretical properties seen at graphene is atomic collapse behaviour of electrons. The first steps through that concept taken when the Dirac equation solved for an electron in a field of a point charge by Darwin(Darwin (1928)) and Gordon(Gordon (1926)). It is seen that for point charges which has greater charge than 137 electrons has, shows no discrete energy spectrum. Here, stable atomic bound states are begins to "dive" into the positron continuum and lifetimes becomes finite(Wang et al. (2013)). As electron wave function component falls toward the nucleus, a positron component escapes to infinity. After that realization the Dirac equation solved for more realistic case: for a field with finite radius, a nucleus! Then, critical value for the observation of atomic collapse found as $Z_{cr} \approx 172$.

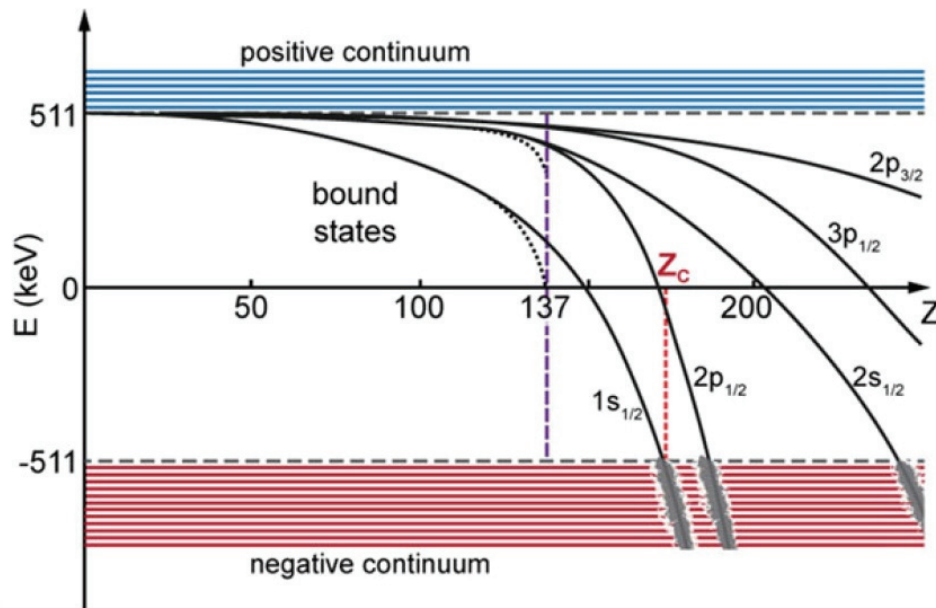


Figure 1.5. Schematic drawing of the atomic bounding energies as function of the atomic number Z and the level diving process in the supercritical regime. The dotted curves indicate the solutions for a point charge while the solid curves take into account the finite size of the nucleus (Source: Moldovan and Peeters (2016))

Because of the nature doesn't serve an atom that much heavy, people tried to obtain that value by colliding heavy ions. Although, positron peaks are observed in that experiments, due to the complexity of the process', that peaks couldn't related to specific positron creation case(Schweppe et al. (1983); Cowan et al. (1985); Soff et al. (1985)). Now, thanks to graphene's large fine structure constant, we are able to observe this phenomena in a small energy scale.

CHAPTER 2

THEORETICAL FOUNDATIONS

In this section we will introduce graphene and examine its electronic behaviour by the first method that been used historically(Wallace (1947)). Then we will also introduce Mean-Field Hubbard model which we'll use for investigating its magnetic effects by including spin property of electrons and electron-electron interactions with this model.

2.1. Tight-Binding Model

Tight-binding method can be considered as the most elementary method to treat crystal structures. Although its simplicity it's very accurate for graphene(Wallace (1947)). In an atom its electrons stack in shells around a nucleus. In a complex structure of atoms, they prefer to create electronic bonds that they can find them in a more stable state. As electronic shells getting closer to be filled the more stable state occurs. Electrons in closed shells(conduction electrons) are less likely to interact compared to in unclosed shells(valence electrons). So, for those "likely to interact" electrons must overcome an energy that occurs from overlapping wave functions with other atoms' electrons in order to disperse along the crystal.

Carbon atoms that forms graphene, has six electrons. Four out of six of them are valence electrons. Normally, a carbon atom has atomic orbital configuration $1s^2 2s^2 2p^2$ in the ground state. But in the formation of graphene structure, three of those valence electrons occupies s , $2p_x$, $2p_y$ orbitals becoming sp^2 hybridized, and creates σ bonds with its neighbour carbon atoms on the plane. Those strong bonds are related to mechanical properties of graphene. The remaining unhybridized electron fills the p_z orbital. This orbital stands perpendicular to the surface and it creates π bond which is the result of the overlapping p_z orbitals of the other carbon atoms. Those bonds determines the electronic features of graphene. The first examination of graphene in 1947, P.R. Wallace studied those electrons in p_z orbitals; in his paper, titled "The Band Theory of Graphite", and he gave highly accurate calculations for graphene although tight-binding model does not take electron-electron interactions into account.

For generating the method, we can write total electronic wave function as super-

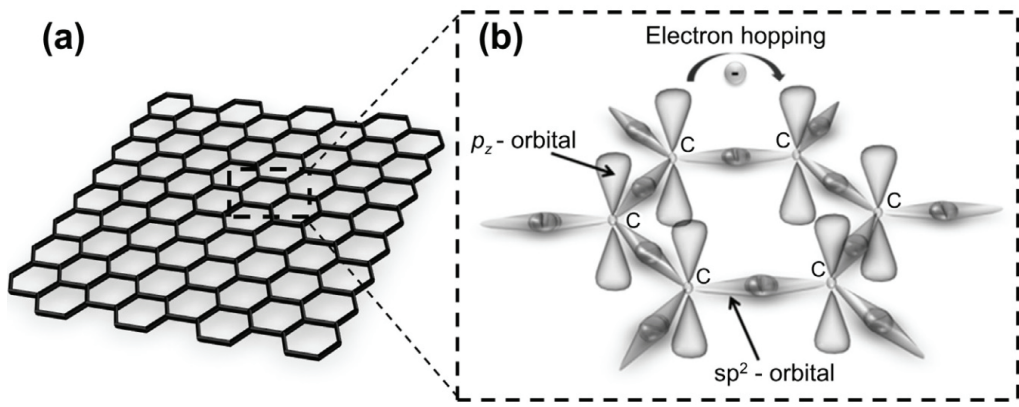


Figure 2.1. (a) Lattice structure of graphene. (b) sp^2 hybridization of carbon atoms to form the 2D crystal structure of graphene as well as delocalized π orbitals. (Source: Liang (2014)).

position of localized orbitals

$$\psi(\vec{r}) = \sum_i C_i \phi_i(\vec{r} - \vec{r}_i) \quad (2.1)$$

By solving time-independent Schrödinger equation we can find the C_i 's,

$$\hat{H}\psi(\vec{r}) = E\psi(\vec{r}) \quad (2.2)$$

We multiply the equation by $\langle \phi_i |$ from the left and then extend it, in terms of localized orbitals.

$$\langle \phi_i | \hat{H} | \psi \rangle - E \langle \phi_i | \psi \rangle = 0 \quad (2.3)$$

$$\sum_n C_n (\langle \phi_i | \hat{H} | \phi_n \rangle - E \langle \phi_i | \phi_n \rangle) = 0 \quad (2.4)$$

At this point, in order to simplify our job, we will only consider about nearest neighbour atoms. Now, summation below only depends on neighbour atoms.

$$\sum_{\langle n,i \rangle} C_n (\langle \phi_i | \hat{H} | \phi_n \rangle - E \langle \phi_i | \phi_n \rangle) = 0 \quad (2.5)$$

where $\langle n, i \rangle$ indicates summation is over nearest neighbour atoms where integrals

$$\langle \phi_i | \hat{H} | \phi_n \rangle = \begin{cases} t & \text{if } i = n \\ 0 & \text{if } i \neq n \end{cases} \quad (2.6)$$

We can use Bloch wavefunctions due to translational symmetry,

$$\psi_k^i(\vec{r}) = \frac{1}{\sqrt{N}} \sum_i e^{i\vec{k}\cdot\vec{r}_i} \phi(\vec{r} - \vec{r}_i) \quad (2.7)$$

In graphene, carbon atoms are in formation of the honeycomb lattice. The unit cell of a honeycomb lattice contains two atoms, A and B, that form triangular Bravais sublattices. Using the Bloch's theorem the wave functions for that sublattices can be written in terms of localized p_z orbitals as,

$$\psi_k^A(r) = \frac{1}{\sqrt{N_A}} \sum_{R_A} e^{ikR_A} \phi_{p_z}(\vec{r} - \vec{R}_A) \quad (2.8)$$

$$\psi_k^B(r) = \frac{1}{\sqrt{N_B}} \sum_{R_B} e^{ikR_B} \phi_{p_z}(\vec{r} - \vec{R}_B) \quad (2.9)$$

where N_A and N_B are the number of A and B sublattice sites, respectively. For graphene, the positions of sublattice R_A and R_B are given as

$$R_A = na_1 + ma_2 + b, \quad (2.10)$$

$$R_B = na_1 + ma_2, \quad (2.11)$$

The total wavefunction can be written as linear combination of two sublattice wavefunc-

tions:

$$\psi_k(r) = A_k \psi_k^A(r) + B_k \psi_k^B(r) \quad (2.12)$$

Plugging the total wavefunction into time independent Schrodinger equation and multiplying from the left side with each sublattice wavefunctions we can get A_k and B_k coefficients.

$$\langle \psi_k^A | H | \psi_k \rangle = \langle \psi_k^A | \psi_k \rangle \quad (2.13)$$

$$\langle \psi_k^B | H | \psi_k \rangle = \langle \psi_k^B | \psi_k \rangle \quad (2.14)$$

Due to neglected on-site energies we have:

$$\langle \psi_k^A | H | \psi_k^A \rangle = 0 \quad (2.15)$$

$$\langle \psi_k^B | H | \psi_k^B \rangle = 0 \quad (2.16)$$

and we left with the off-site hopping integrals with only nearest neighbour hopping parameters included,

$$\langle \psi_k^B | H | \psi_k^A \rangle = \frac{1}{N} \sum_{\langle R_A, R_B \rangle} e^{ik(R_A - R_B)} \int dr \phi_z^*(r - R_B) H(r - R_B) \phi_z(r - R_A) \quad (2.17)$$

here, the integral is a constant and will be shown as t further. If the summation expanded over the three nearest neighbour, equation 2.17 can be written as,

$$\langle \psi_k^B | H | \psi_k^A \rangle = t(e^{-ikb} + e^{(-ik(b-a_1)} + e^{(-ik(b-a_2)})) \quad (2.18)$$

$$= tf(\mathbf{k}) \quad (2.19)$$

Here, lattice vectors for graphene defined as,

$$a_1 = \frac{a}{2}(\sqrt{3}, 3), \quad a_2 = \frac{a}{2}(-\sqrt{3}, 3) \quad \text{and} \quad b = a(0, 1) \quad (2.20)$$

Knowing that,

$$\langle \psi_k^B | H | \psi_k^A \rangle^* = \langle \psi_k^A | H | \psi_k^B \rangle \quad (2.21)$$

We can write the problem that reduced to eigenvalue problem in matrix form,

$$E(\mathbf{k}) \begin{pmatrix} A_k \\ B_k \end{pmatrix} = t \begin{pmatrix} 0 & f(\mathbf{k}) \\ f(\mathbf{k})^* & 0 \end{pmatrix} \begin{pmatrix} A_k \\ B_k \end{pmatrix} \quad (2.22)$$

And its eigenvalues are,

$$E_{\pm}(\mathbf{k}) = \pm |t f(\mathbf{k})| \quad (2.23)$$

which corresponds to the spinors below,

$$\begin{pmatrix} A_k \\ B_k \end{pmatrix} = \frac{1}{\sqrt{2}} \begin{pmatrix} 1 \\ \frac{\pm f^*(\mathbf{k})}{|f(\mathbf{k})|} \end{pmatrix} \quad (2.24)$$

Note that the spectrum is gapless at six points in the first Brillouin zone and there is a symmetry with respect to the Fermi level ($E_F = 0$). However this symmetry is broken if the next nearest neighbours are taken into account. Two of these six corners, indicated by \mathbf{K} and \mathbf{K}' , are non-equivalent and the other four points can be obtained by a translation by reciprocal vectors. Other high symmetry points of reciprocal space are; the Γ point in the center of the Brillouin zone and the \mathbf{M} point which is between the closest \mathbf{K} and \mathbf{K}' points (Guclu (2014)). While examining electronic properties, we

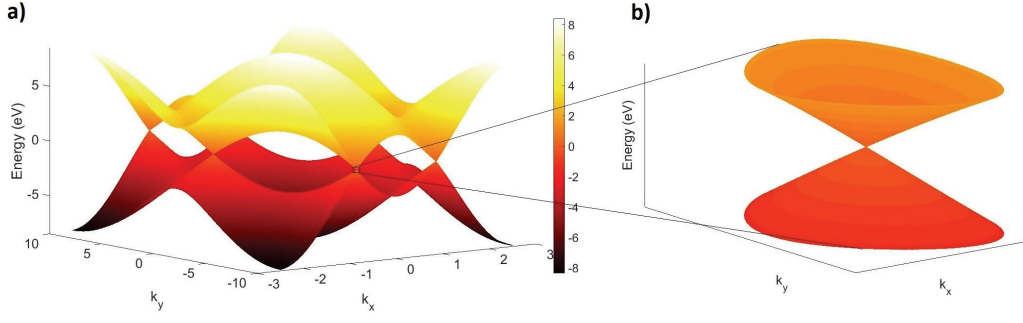


Figure 2.2. (a) Band structure of Graphene, (b) Closeup to Fermi Level.

expand energy dispersion $E(\mathbf{k})$ in Taylor series around \mathbf{K} and \mathbf{K}' points,

$$f(\mathbf{K} + \mathbf{q}) = f(\mathbf{K}) + f'(\mathbf{K})\mathbf{q} \quad (2.25)$$

which \mathbf{q} is a small vector taken respect to \mathbf{K} point.

$$\begin{aligned} f(\mathbf{K} + \mathbf{q}) &= (e^{-i\mathbf{K}b} + e^{-i\mathbf{K}(b-a_1)} + e^{-i\mathbf{K}(b-a_2)}) \\ &\quad - [i\mathbf{q}b e^{-i\mathbf{K}b} + i\mathbf{q}(b-a_1)e^{-i\mathbf{K}(b-a_1)} + i\mathbf{q}(b-a_2)e^{-i\mathbf{K}(b-a_2)}] \\ &= (1 - i\mathbf{q}b)[e^{-i\mathbf{K}b} + e^{-i\mathbf{K}(b-a_1)} + e^{-i\mathbf{K}(b-a_2)}] \\ &\quad + [i\mathbf{q}a_1 e^{-i\mathbf{K}(b-a_1)} + i\mathbf{q}a_2 e^{-i\mathbf{K}(b-a_2)}] \end{aligned} \quad (2.26)$$

here $\mathbf{K} = (\frac{4\pi}{3}\sqrt{3}a, 0)$ and by putting the other vectors,

$$\begin{aligned} f(\mathbf{K} + \mathbf{q}) &= (1 - i\mathbf{q}b) \underbrace{[1 + e^{\frac{2\pi i}{3}} + e^{-\frac{2\pi i}{3}}]}_{=0} + \left[i \left(-\frac{1}{2} + i\frac{\sqrt{3}}{2} \right) a \left(\mathbf{q}_x \frac{\sqrt{3}}{2} + \frac{3}{2} \mathbf{q}_y \right) \right. \\ &\quad \left. + i \left(-\frac{1}{2} + i\frac{-\sqrt{3}}{2} \right) a \left(-\mathbf{q}_x \frac{\sqrt{3}}{2} + \frac{3}{2} \mathbf{q}_y \right) \right] \\ &= \frac{3}{2} a (-\mathbf{q}_x, -i\mathbf{q}_y) \end{aligned} \quad (2.27)$$

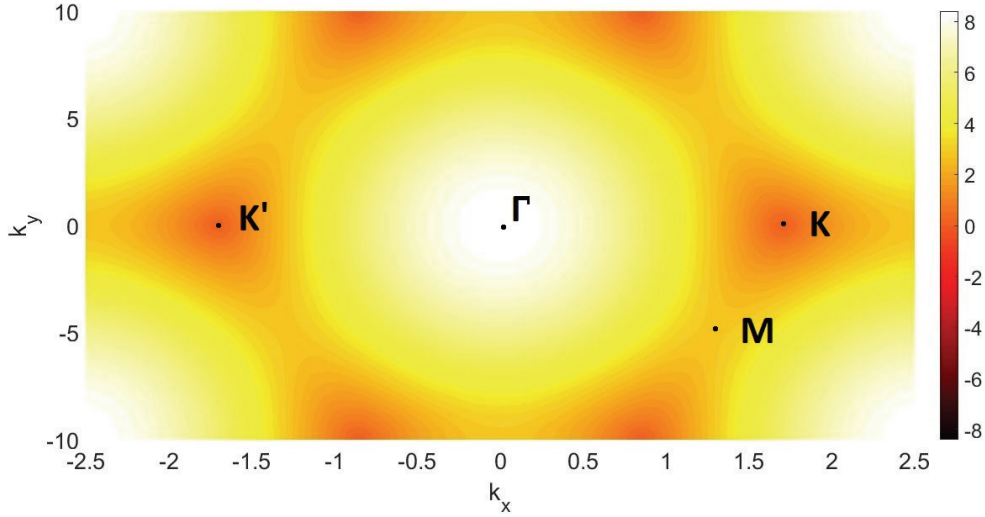


Figure 2.3. Symmetry points of Graphene.

then, equation 2.24 can then be written as

$$E_K(\mathbf{q}) = \begin{pmatrix} A_{\mathbf{q}} \\ B_{\mathbf{q}} \end{pmatrix} = -\frac{3}{2}ta \begin{pmatrix} 0 & \mathbf{q}_x - i\mathbf{q}_y \\ \mathbf{q}_x + i\mathbf{q}_y & 0 \end{pmatrix} \begin{pmatrix} A_{\mathbf{q}} \\ B_{\mathbf{q}} \end{pmatrix} \quad (2.28)$$

Eigenenergies and corresponding eigenfunctions are,

$$E_K^c(\mathbf{q}) = \pm \frac{3}{2}a|t||\mathbf{q}|, \quad (2.29)$$

$$\psi_K^c(\mathbf{q}) = \frac{1}{\sqrt{2}} \begin{pmatrix} e^{-i\theta_{\mathbf{q}}/2} \\ \pm e^{i\theta_{\mathbf{q}}/2} \end{pmatrix} \quad (2.30)$$

\pm signs for a conduction and valence band, respectively. Same calculations can be done around point K' for small \mathbf{q} , and we get same eigenenergies and eigenvectors. By introducing a Fermi velocity $v_F = \frac{3ta}{2\hbar}$, we can write equation (2.29) as

$$E(\mathbf{q}) = \pm \hbar v_F |\mathbf{q}| \quad (2.31)$$

This solution is identical to the solution of the Dirac Hamiltonian for relativistic massless

fermions. Here, a speed of light is played by a Fermi velocity. One can estimate $v_F \approx 10^6 m/s$ which is 300 times smaller than a speed of light. Two eigenfunctions for \mathbf{K} and \mathbf{K}' points of spinor wave functions for fermions. Here, a role of spin is played by wave functions of two sublattices, A and B. Because of that, they called as pseudospins and can be described by Pauli matrices $\sigma = (\sigma_x, \sigma_y, \sigma_z)$. Thus, the eigenfunctions given by equation 2.30 are usually called pseudospinor. (Guclu (2014)).

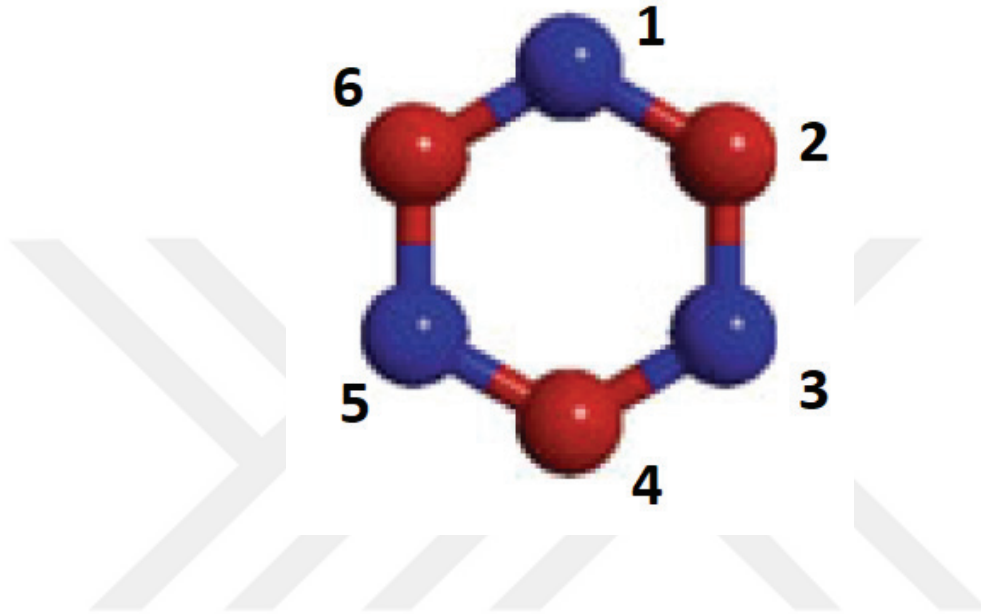


Figure 2.4. A benzene ring(Source: Guclu (2014)).

Easiest way to describe TB hamiltonian is using second-quantization notation:

$$H_{TB} = \sum_{\langle ij \rangle} \sum_{\sigma} t_{ij} (c_{i\sigma}^{\dagger} c_{j\sigma} + h.c.) \quad (2.32)$$

Here, $c_{j\sigma}$ is the annihilation operator which annihilates an electron from the j site with spin σ , and the $c_{i\sigma}^{\dagger}$ creates the same electron on i site with hopping energy $t_{ij} = -2.8$ eV(Castro Neto et al. (2009)). $\langle ij \rangle$ indicates that we are considering only the nearest neighbour hoppings. In the further calculations we'll also include second nearest neighbour hopping energy.

A simple example about how a TB Hamiltonian appears can be shown by modelling a benzene ring(Fig. 2.4). Here, the electron on site 1 can hop to only 2nd and 6th sites. The the electron on site 2 can hop to only 1st and 3rd sites, and goes on. The TB

Hamiltonian in matrix form appears as,

$$H_{TB_{benzene}} = \begin{bmatrix} 0 & t & 0 & 0 & 0 & t \\ t & 0 & t & 0 & 0 & 0 \\ 0 & t & 0 & t & 0 & 0 \\ 0 & 0 & t & 0 & t & 0 \\ 0 & 0 & 0 & t & 0 & t \\ t & 0 & 0 & 0 & t & 0 \end{bmatrix} \quad (2.33)$$

2.2. Mean-Field Hubbard Model

While using TB model, we totally ignored spin dependence and electronic correlation effects. Because of that, we cannot expect to investigate magnetic properties of the system. Hubbard method is a simplified instrument to investigate ferromagnetism, it neglects n-fold degeneracy of any orbital that valence electrons are in and defines the orbitals as a half-filled s orbital (Eder (2017)). Foreseeingly, finding out that the Hubbard model is nothing but TB model with an extra electron-electron interaction term, won't be surprising. Now, starting from exact many-bond Hamiltonian written in second quantization formalism we are going to derive Hubbard Hamiltonian and Mean-Field Hubbard Hamiltonian further.

$$H = \sum_{pq} t_{pq} c_p^\dagger c_q + \frac{1}{2} \sum_{pqrs} (pq|V|rs) c_p^\dagger c_q^\dagger c_r c_s \quad (2.34)$$

For the first term, where $p = i\sigma$, $q = j\sigma'$ and σ indicates spin dependence.

$$t_{pq} = \langle p|t|q \rangle = \langle i\sigma|t|j\sigma' \rangle = \langle i|t|j \rangle \underbrace{\langle \sigma|\sigma' \rangle}_{\delta_{\sigma\sigma'}} \quad (2.35)$$

Similarly for interaction term, $p = i\sigma$, $p = j\sigma'$, $r = k\sigma''$, $s = l\sigma'''$

$$V_{i,j} = \frac{1}{2} \sum_{pqrs} (pq|V|rs) c_p^\dagger c_q^\dagger c_r c_s = \frac{1}{2} \sum_{ijkl} \langle ij|V|kl \rangle c_i^\dagger c_j^\dagger c_k c_l \underbrace{\langle \sigma|\sigma''' \rangle}_{\delta_{\sigma\sigma'''}} \underbrace{\langle \sigma'|\sigma'' \rangle}_{\delta_{\sigma'\sigma''}} \quad (2.36)$$

Finally, equation (2.34) can be written as,

$$H = \sum_{ij} t_{ij} c_i^\dagger c_j + \frac{1}{2} \sum_{ijkl} \langle ij|V|kl \rangle c_i^\dagger c_j^\dagger c_k c_l \langle \sigma|\sigma''' \rangle \langle \sigma'|\sigma'' \rangle \quad (2.37)$$

Next, to calculate on-site repulsion term saying that

$$\langle ii|V|ii \rangle = U \quad (2.38)$$

$$\frac{1}{2} \sum_{ijkl} \langle ij|V|kl \rangle c_{i\sigma}^\dagger c_{i\sigma'}^\dagger c_{i\sigma'} c_{i\sigma} = \frac{1}{2} \sum_{i\sigma\sigma'} U c_{i\sigma}^\dagger c_{i\sigma'}^\dagger c_{i\sigma'} c_{i\sigma} \quad (2.39)$$

After expanding the spin terms and exploiting the second quantization algebra, final on site expression becomes,

$$\frac{U}{2} \sum_i \underbrace{c_{i\uparrow}^\dagger c_{i\uparrow}}_{n_{i\uparrow}} \underbrace{c_{i\downarrow}^\dagger c_{i\downarrow}}_{n_{i\downarrow}} + c_{i\downarrow}^\dagger c_{i\downarrow} c_{i\uparrow}^\dagger c_{i\uparrow} = U \sum_i n_{i\uparrow} n_{i\downarrow} \quad (2.40)$$

Likewise for off-site repulsion term,

$$\langle ji|V|ij \rangle = V_{ij} \quad \text{and} \quad \frac{1}{2} \sum_{\substack{i \neq j \\ \sigma\sigma'}} \langle ji|V|ij \rangle c_{i\sigma}^\dagger c_{i\sigma'}^\dagger c_{i\sigma'} c_{i\sigma} \quad (2.41)$$

It is necessary to convert our quartic hamiltonian into a quadratic one because handling a quartic hamiltonian is almost impossible even for a computational power. Again using the properties $\{c_{i\sigma}, c_{j\sigma}\} = 0$ and $\{c_{j\sigma'}^\dagger, c_{i\sigma}\} = \delta_{i,j} \delta_{\sigma,\sigma'}$, and also converting suitable products

of creating and annihilation operators into number operators; we get,

$$\begin{aligned}
\frac{1}{2} \sum_{\substack{i \neq j \\ \sigma \sigma'}} V_{ij} c_{i\sigma}^\dagger c_{j\sigma'} (-c_{i\sigma}^\dagger c_{j\sigma'}) &= \frac{1}{2} \sum_{\substack{i \neq j \\ \sigma \sigma'}} V_{ij} c_{i\sigma}^\dagger (-\delta_{\sigma\sigma'} \underbrace{\delta_{ij}}_{\substack{=0 \\ i \neq j}} + c_{i\sigma} c_{j\sigma'}^\dagger) c_{j\sigma'} \\
&= \frac{1}{2} \sum_{\substack{i \neq j \\ \sigma \sigma'}} V_{ij} n_{i\sigma} n_{j\sigma'} \\
&= \frac{1}{2} \sum_{\substack{i \neq j \\ \sigma \sigma'}} V_{ij} (n_{i\uparrow} n_{j\uparrow} + n_{i\downarrow} n_{j\downarrow} + n_{i\uparrow} n_{j\downarrow} + n_{i\downarrow} n_{j\uparrow}) \\
&= \frac{1}{2} \sum_{\substack{i \neq j \\ \sigma \sigma'}} V_{ij} \underbrace{(n_{i\uparrow} n_{i\downarrow})}_{n_i} \underbrace{(n_{j\uparrow} n_{j\downarrow})}_{n_j} = \frac{1}{2} \sum_{\substack{i \neq j \\ \sigma \sigma'}} V_{ij} n_i n_j
\end{aligned} \tag{2.42}$$

Finally Hubbard and extended Hubbard Hamiltonian can be written as summation of all terms.

$$H = \underbrace{\sum_{\substack{ij \\ \sigma}} t_{ij} c_{i\sigma}^\dagger c_{j\sigma}}_{\text{Hubbard Model}} + U \sum_i n_{i\uparrow} n_{i\downarrow} + \frac{1}{2} \sum_{i \neq j} V_{ij} n_i n_j \tag{2.43}$$

Extended Hubbard Model

Now, we can make some comments on the model by looking closely. The first term is the TB term in second quantization form. It represents electrons' moving from one site with hopping energy t . The second term is for on-site Coulomb repulsion that prevents us to putting two electrons with opposite spin in same site, by costing it with raising the system's energy, which is less favorable if we want to find ground state energy for a system. Actually, putting opposite spins in same site lowers the energy but, because of number of intracting electrons equal to number of sites for graphene, keeping them in different sites is more favorable in order to lower the total energy. The third term is off-site Coulomb repulsion term that includes the interaction energy of the electrons on different sites. Also one can notice that there is no term related to putting electrons with same spin on same site in accordance with the Pauli exclusion principle.

Now that the exact Hamiltonian is derived, we can begin derivation of mean-field Hubbard Hamiltonian. Now we are going to assume that, system interacts with a constant background charge field and to do so we begin by expressing the number operators as an

average value plus a deviation from the average:

$$n_{i\uparrow} = \langle n_{i\uparrow} \rangle + \underbrace{(n_{i\uparrow} - \langle n_{i\uparrow} \rangle)}_{\Delta n_{i\uparrow}} \quad \text{and} \quad n_{i\downarrow} = \langle n_{i\downarrow} \rangle + \underbrace{(n_{i\downarrow} - \langle n_{i\downarrow} \rangle)}_{\Delta n_{i\downarrow}} \quad (2.44)$$

$$n_{i\sigma} = \langle n_{i\sigma} \rangle + \underbrace{(n_{i\sigma} - \langle n_{i\sigma} \rangle)}_{\Delta n_{i\sigma}} \quad \text{and} \quad n_{j\sigma} = \langle n_{j\sigma} \rangle + \underbrace{(n_{j\sigma} - \langle n_{j\sigma} \rangle)}_{\Delta n_{j\sigma}} \quad (2.45)$$

For on-site term using equation (2.44),

$$\begin{aligned} n_{i\uparrow}n_{i\downarrow} &= [\langle n_{i\uparrow} \rangle + \Delta n_{i\uparrow}][\langle n_{i\downarrow} \rangle + \Delta n_{i\downarrow}] \\ &= \langle n_{i\uparrow} \rangle \langle n_{i\downarrow} \rangle + \langle n_{i\uparrow} \rangle \Delta n_{i\downarrow} + \Delta n_{i\uparrow} \langle n_{i\downarrow} \rangle + \underbrace{\Delta n_{i\uparrow} \Delta n_{i\downarrow}}_{\approx 0} \\ &\approx \langle n_{i\uparrow} \rangle n_{i\downarrow} + \langle n_{i\downarrow} \rangle n_{i\uparrow} - \langle n_{i\uparrow} \rangle \langle n_{i\downarrow} \rangle \end{aligned} \quad (2.46)$$

By using equation (2.45) similar to preceding calculation off-site repulsion term becomes,

$$n_i n_j \approx \langle n_i \rangle n_j + \langle n_j \rangle n_i - \langle n_i \rangle \langle n_j \rangle \quad (2.47)$$

Finally Hamiltonian can be approximated by,

$$\begin{aligned} H &\approx \sum_{\substack{ij \\ \sigma}} t_{ij} c_{i\sigma}^\dagger c_{j\sigma}^\dagger + U \sum_i \langle n_{i\uparrow} \rangle n_{i\downarrow} + \langle n_{i\downarrow} \rangle n_{i\uparrow} - \langle n_{i\uparrow} \rangle \langle n_{i\downarrow} \rangle \\ &\quad + \frac{1}{2} \sum_{i \neq j} V_{ij} \langle n_i \rangle n_j + \langle n_j \rangle n_i - \langle n_i \rangle \langle n_j \rangle \end{aligned} \quad (2.48)$$

Our Hamiltonian is now in quadratic form in the mean-field approximation, and it makes the diagonalization easier. Now we'll take average value of an p_z orbital as 1 for a charge neutral system and also average value of a spin as 1/2 for both up and down spin; for

considering the bulk graphene.

$$\langle n_i \rangle = 1 \quad \text{and} \quad \langle n_{i\sigma} \rangle = \frac{1}{2} \quad (2.49)$$

which makes bulk mean field Hamiltonian,

$$H_{MF}^{Bulk} = \sum_{ij, \sigma} t_{ij} c_{i\sigma}^\dagger c_{j\sigma} + \frac{U}{2} \sum_i (n_{i\uparrow} n_{i\downarrow} - \frac{1}{2}) + \frac{1}{2} \sum_{ij} V_{ij} (n_i + n_j - 1) \quad (2.50)$$

To get the single body mean field Hubbard Hamiltonian, we are going to use

$$\begin{aligned} H_{MF} &= H_{MF} - H_{MF}^{Bulk} + H_{MF}^{Bulk} \\ &= \sum_{ij, \sigma} t_{ij} c_{i\sigma}^\dagger c_{j\sigma} + U \sum_i \langle n_{i\uparrow} \rangle n_{i\downarrow} + \langle n_{i\downarrow} \rangle n_{i\uparrow} - \langle n_{i\uparrow} \rangle \langle n_{i\downarrow} \rangle \\ &\quad + \frac{1}{2} \sum_{i \neq j} V_{ij} \langle n_i \rangle n_j + \langle n_j \rangle n_i - \langle n_i \rangle \langle n_j \rangle \\ &\quad - \sum_{ij, \sigma} t_{ij} c_{i\sigma}^\dagger c_{j\sigma} + \frac{U}{2} \sum_i (n_{i\uparrow} n_{i\downarrow} - \frac{1}{2}) + \frac{1}{2} \sum_{ij} V_{ij} (n_i + n_j - 1) \\ &\quad + \sum_{ij, \sigma} t_{ij} c_{i\sigma}^\dagger c_{j\sigma} + \frac{U}{2} \sum_i (n_{i\uparrow} n_{i\downarrow} - \frac{1}{2}) + \frac{1}{2} \sum_{ij} V_{ij} (n_i + n_j - 1) \\ &= \underbrace{\sum_{ij, \sigma} t_{ij} c_{i\sigma}^\dagger c_{j\sigma} + \frac{U}{2} \sum_i (n_{i\uparrow} n_{i\downarrow}) + \frac{1}{2} \sum_{ij} V_{ij} (n_i + n_j)}_{\sum_{\langle ij \rangle, \sigma} \tau_{ij} (c_{i\sigma}^\dagger c_{j\sigma} + h.c.)} \\ &\quad + U \sum_i [(\langle n_{i\uparrow} \rangle - \frac{1}{2}) n_{i\downarrow} + (\langle n_{i\downarrow} \rangle - \frac{1}{2}) n_{i\uparrow}] \\ &\quad + \frac{1}{2} \sum_{ij} V_{ij} [(\langle n_i \rangle - \frac{1}{2}) n_j + (\langle n_j \rangle - \frac{1}{2}) n_i] + \text{Constants} \end{aligned} \quad (2.51)$$

Finally knowing that $V_{ij} = V_{ji}$, mean field Hamiltonian becomes its last form as follow.

$$\begin{aligned}
H_{MFH} = & \sum_{\substack{ij \\ \sigma}} \tau_{ij} (c_{i\sigma}^\dagger c_{j\sigma}^\dagger + h.c.) + U \sum_i (\langle n_{i\uparrow} \rangle - \frac{1}{2}) n_{i\downarrow} + (\langle n_{i\downarrow} \rangle - \frac{1}{2}) n_{i\uparrow} \\
& + \frac{1}{2} \sum_{ij} V_{ij} [(\langle n_i \rangle - 1) n_j + (\langle n_j \rangle - 1) n_i]
\end{aligned} \tag{2.52}$$

2.3. Further Calculation Details

Before discussing the results, some calculation details should be given. For all calculations both for Tight-Binding and mean-field Hubbard method, hopping parameters are taken as $t=-2.8$ eV for the nearest neighbors and $t_{nnn}=0$ eV and $t_{nnn}=-0.1$ eV for the second nearest neighbors (Castro Neto et al. (2009)). Because of vagueness of fermi level for the spatially non-symmetric vacancy modellings on the dots, calculations made by taking $t_{nnn}=0$ eV and $t_{nnn}=-0.1$ eV and are given together. On site Coulomb interaction term U is taken to be $16.522/\kappa$ where κ is effective dielectric constant and can be changed for the desired substrate. For the long-range off-site Coulomb interactions V_{ij} are taken as $8.64/\kappa$ and $5.33/\kappa$ for the first and the second nearest neighbours respectively and $1/d_{ij}$ for other distant atoms. All interaction integrals are calculated by considering Slater π_z orbitals.

MFH problems are solved self consistently because of there is no formal wavefunctions for MFH problem. In this process, we used eigenfunctions of TB hamiltonian with additional initial conditions to attract electrons around the centers of the Coulomb potential applied at the first step. End of the every self consistent loop we checked that how much the current ground state smaller from the previous one and used their differences as a cut-off for a small value (check if $abs(GSE(n) - (GSE(n-1))) \leq 10^{-10}$). Also with different weight adjustments for wavefunctions between the self consistent calculation steps, we provide proper conditions in order to minimise the step number and to get proper ground state energy at the same time. For example, we took 40 percent of the previous wavefunction and 60 percent of the current. To do so, we prohibited divergence from the ground state energy.

CHAPTER 3

DISORDERS AND GRAPHENE

In this chapter we will categorize possible disorder types can be found on graphene and discuss theoretical foundations how graphene's electronic properties change related to defects generally.

3.1. Absence of Backscattering

The analytical calculations show that long-range potential which ranges more than the lattice constant, vanishes the probability of backscattering by making effective potential same both A and B sublattices(Ando and Nakanishi (1998)). In other words, the conserved symmetry of sublattices causes destructive interference between scattering waves. This makes graphene highly conductive.

3.2. Long-Range Disorder

Graphene products can be disordered due to the surface atoms of the substrate that it putten on, and we will consider those kind of disorders as long-range disorder. Physically, if the potential range is larger than the lattice constant but much smaller than the typical electron wavelength we call that type of disorders as long-range disorders(Ando et al. (2002)) . In order to model the long-range disorder due to the potential fluctuations by the substrate, we can use a superposition of gaussian electrostatic potential. The long-range disorders can cause a magnetic phase transition. Also, if the disorder has a long-range character, it can lead to charge localizations as electron-hole puddles(Altintas et al. (2017)).

3.3. Short-Range Disorders

Examples of this types of disorder arises because of localised defects such as vacancies, F centres, interstitials, substitutional impurity atoms, di-vacancies, dislocations.

By modelling a short-range disorder, a Dirac-delta potential can be considered at the disorder center. For short range disorders, scattering potential is smaller than the lattice constant of graphene(Ando et al. (2002)). In our work our defects are in vacancy type. A vacancy can be described as absence of an atom on the lattice. Vacancies are mostly produced by post-synthesis process like knock-on events by high energy electron, ion, or neutron radiation can dislodge or fully remove a carbon atom(Collins (2009)). In weakly-bonded metal crystals an absence of an atom can be considered as a small perturbation. But for graphene it's not the case. When a graphene vacancy breaks σ bonds, the energy must be considered around 7.8 eV(Kaxiras and Pandey (1988)). Vacancies result with three dangling bonds that will interact or rehybridize with surrounding molecules or atoms. The lattice defects break the lattice symmetry. This broken symmetry causes a local magnetic moment in a small site around the defect. Therefore, one can induce a local magnetism in graphene by introducing the lattice defects.

3.4. Supercritical Disorders

After derivation of the Schrödinger's equation(Schrodinger (1926)) for quantum mechanical systems, theorists tried to derive an equation for the relativistic particles which are already has quantum mechanical properties(Klein (1927); Gordon (1926); Dirac and Fowler (1928a,b)). In 1928 P. A. M. Dirac derived that equation which is know by his name, as stated below,

$$\left(\beta mc^2 + c\left(\sum_{n=1}^3 \alpha_n p_n\right)\right)\psi(x, t) = i\hbar \frac{\partial \psi(x, t)}{\partial t} \quad (3.1)$$

Here, α and β are corresponds to,

$$\alpha_n = \begin{pmatrix} 0 & \sigma_n \\ \sigma_n & 0 \end{pmatrix} \quad \text{and} \quad \beta = \begin{pmatrix} \mathbb{1} & 0 \\ 0 & \mathbb{1} \end{pmatrix} \quad (3.2)$$

where

$$\sigma_1 = \begin{pmatrix} 0 & 1 \\ 1 & 0 \end{pmatrix}, \quad \sigma_2 = \begin{pmatrix} 0 & -i \\ i & 0 \end{pmatrix}, \quad \sigma_3 = \begin{pmatrix} 1 & 0 \\ 0 & -1 \end{pmatrix} \quad (3.3)$$

are Pauli spin matrices. Solution of Dirac equation proposed negative energy values. Dirac explained that by thinking as all of the negative energy states are already filled with electrons and if one of those electrons kicked out by help of external energy, let say photons, it leaves a "hole" behind with positive charge(Dirac and Fowler (1930)). Then the "holes", that we recognise as positrons today, are discovered experimentally by Carl D. Anderson in 1933(Anderson (1933)). After derivation of the equation, Darwin(Darwin (1928)) and Gordon(Gordon (1926)) tested it with a special potential $V(r) = -Z\alpha/r$ and reached Sommerfeld formula for a hydrogenic atom(Sommerfeld (1919)) which is,

$$E = \frac{mc^2}{\left[1 + \frac{(Z\alpha)^2}{\sqrt{(j+1/2)^2 - (Z\alpha)^2} + n}\right]} \quad (3.4)$$

Here $\alpha = \frac{1}{137}$ is fine structure constant, j is total angular momentum and n is quantum number. If we look closer, we can see that states with total angular momentum j=1/2 gives imaginary values while $1 > Z\alpha$. So that is making $Z = 137$ is a critical value for a point like nucleus for Dirac equation. For example $1s_{1/2}$ energy is calculated by

$$E_{1s_{1/2}} = mc^2 \sqrt{1 - (Z\alpha)^2}, \quad (3.5)$$

which becomes zero at $Z = 137$ and the slope of the curve $E_{1s_{1/2}}(Z)$

$$\frac{dE_{1s_{1/2}}(Z)}{dZ} = -mc^2 \frac{Z\alpha}{\sqrt{1 - (Z\alpha)^2}} \quad (3.6)$$

which goes to infinity as Z goes to 137 and offered wavefunctions at small distances begins to oscillate near the origin and loses its physical meaning. Electron states goes into positron states when the atomic number changes from sub-critical to supercritical. Which brings us break down of the wavefunction what is called as "atomic collapse". Because

of the point charge description of atom is far from being physical, an investigation of finite radius solution needed(Pomeranchuk and Smorodinsky (1945); Werner and Wheeler (1958); Pieper and Greiner (1969)). In a tiduous examination made by Soff et. al it is calculated as $Z_{cr} \approx 172$ (Soff and Rafelski (Soff and Rafelski)).

Ofcourse, Z_{cr} is much higher atomic number than natural atoms can have. In order to obtain the effects of those superheavy atoms, the collision of heavy ions idea arose. However, experimens and theoretical calculations leded to spontaneous positron emission, the actual source of those emissions cannot be clearly explained(Schweppe et al. (1983); Cowan et al. (1985); Soff et al. (1985)). Thanks to massless Dirac fermions at graphene with Fermi velocity $v_F \approx c/300$ we can investigate atomic collapse physics much smaller energy scale and in two dimensions(Vafek and Vishwanath (2014)). Considering Fermi velocity at graphene we define an effective fine-structure constant as,

$$\alpha = \frac{e^2}{\hbar v \kappa} \approx \frac{2.19}{\kappa} \quad (3.7)$$

where κ is the dielectric constant. Because this effective fine-structure constant will be much higher than the original one, Z_{cr} needed can be taken much smaller(Shytov et al. (2007, 2008)). That means even a charged impurity composed from an element with a small atomic number can be used to observe atomic collapse. So, using graphene changes the energy scale from MeV to sub-eV(Moldovan and Peeters (2016)). The new challange was the observe this effect experimentally. Atomic collapse demonstrated on graphene by using Ca dimmers(Fig. 3.1) at a temperature about absolute zero(Wang et al. (2013); Moldovan and Peeters (2016)).

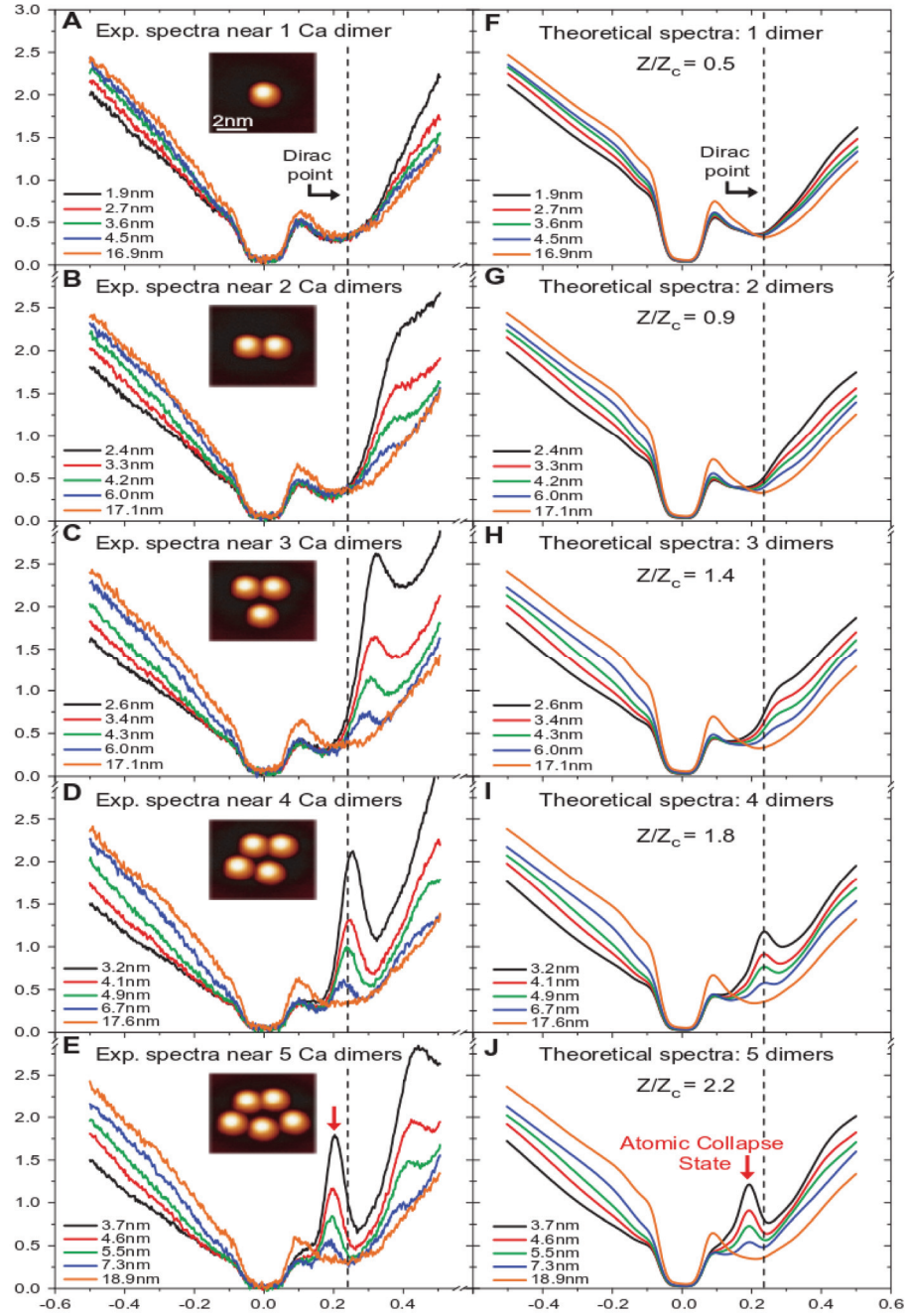


Figure 3.1. Evolution of charged impurity clusters from subcritical to supercritical regime. (A to E) dI/dV spectra measured at different distances from the center of Ca dimer clusters (i.e., artificial nuclei) composed of one to five dimers. (F to J) Theoretical normalized dI/dV spectra (obtained from the Dirac equation) for graphene at the same distances from dimer clusters as in (A) to (E). (Source: Wang et al. (2013))

CHAPTER 4

DEFECT EFFECTS IN GQDS

In this chapter we'll investigate, single and double defect effects. First, by placing a tunable impurity at the center of a GQD we'll examine how the electronic states behave using Tight-Binding and Mean-Field Hubbard model. Then we'll place a vacancy near the center for the same purpose and also use this system to gradually introduce the magnetic behaviour on the GQD. Second, by placing two vacancies in GQDs, we'll observe how its magnetic behaviour change due to distance and the beta value. Then we'll try to understand that how its magnetic behaviour changes using physical concepts.

4.1. Single Defect Effects

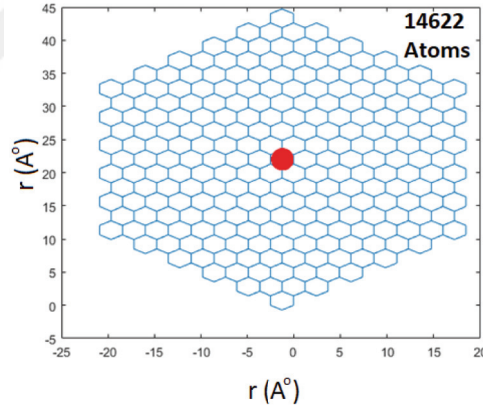


Figure 4.1. Visualization of applied potential with a cut-off area (red area) on hexagonal GQD with armchair edge.

To demonstrate effect of a charged impurity, we modified that Coulomb potential with a decaying length, it becomes,

$$V(r) = \begin{cases} -\hbar v_F \frac{\beta}{r_0} & \text{if } r \leq 1.42 \text{ \AA} \\ -\hbar v_F \frac{\beta}{r} & \text{if } r > 1.42 \text{ \AA} \end{cases} \quad (4.1)$$

where $r_0 = 1.42\text{\AA}$ is the lattice constant and the β (beta) is a dimensionless constant that we're going to use for tune the potential. This kind of supercritical potential has been demonstrated by pushing five Calcium dimers in a place as a cluster at low temperature $T < 10K$.

We calculated eigenenergies for a GQD(14622 Atoms) with armchair edges by using TB method, considering it has an applied Coulomb potential shown in equation (4.1) at the center of the dot without a second nearest neighbour hopping term. A toy model of the system is shown in the Fig. (4.1).

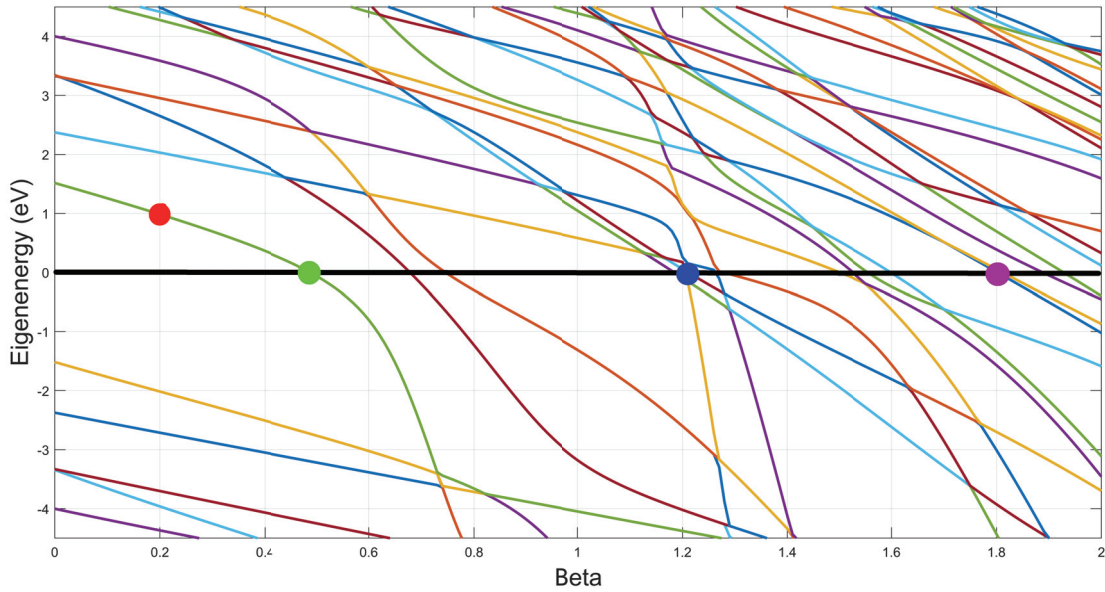


Figure 4.2. TB eigenenergies vs beta for armchair edged hexagonal GQD(14622 Atoms) with snne=0 eV

To examine the behaviour of the electrons under different potential strengths, we varied the beta value from 0 to 2, by raising it 0.1 at every step(Fig. 4.2). The first thing we can observe is the totally symmetric distribution of the energy levels at beta=0 due to absence of the Coulomb potential. Then, the energy levels begin to decrease while the Coulomb potential increase. We see that the first atomic collapse behaviour occurs at beta=0.5 for the first energy state above the fermi level. At this point the Coluomb potential induces an energy about $1.44 \times e^{19}$ eV. That is less than the energy needed to power a single 100 watt light bulb for one second. This value supports our "low energy scale" argument. We also marked the other crucial points which are helping the examine distinct wave function behaviours.

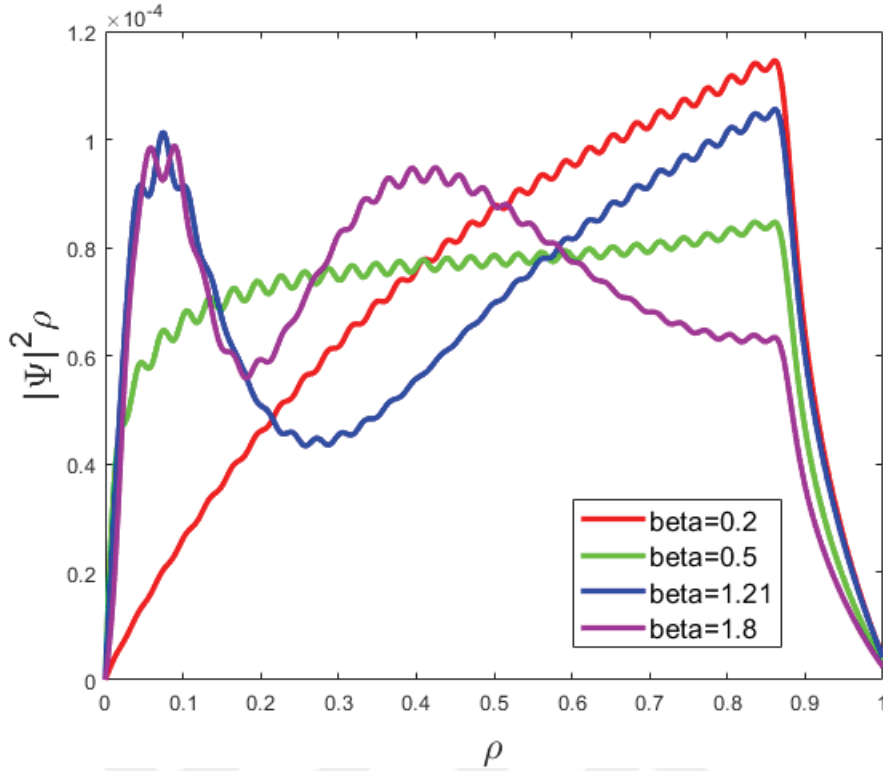


Figure 4.3. Corresponding probability densities for specific beta values pointed in Fig. (4.2) versus $\rho = r/R$.

Fig. 4.3 describes the probability density of electronic states marked in previous Fig. 4.2 versus the unitless distance $\rho = r/R$ to the Coulomb potential. Here r stands for a distance of any position on the GQD from the Coulomb potential that stands on the center of the dot; and R stands for the longest distance from the Coulomb potential. We can see that at $\beta=0.20$ (red line), there is almost no probability of finding electron close around the Coulomb potential. Starting with $\beta=0.50$ (green line), probability distributes evenly, which is the point that we observe the first collapsing event. Then probability of finding the related electron is getting higher and higher due to β , around the Coulomb potential.

Wave functions that belong to the analytic solution for the finite-size impurity has $e^{-2i\sqrt{(Z\alpha)^2 - j^2} \log \rho}$ factor (Van Pottelberge et al. (2017)). That function shows a strict behaviour which is fast oscillations at very close points to the impurity, when the charge is increased. This is a sign for the atomic collapse for us. We can clearly observe that behaviour in Fig. 4.3 at $\beta=1.21$ (blue line) and $\beta=1.80$ (purple line) for related electronic states.

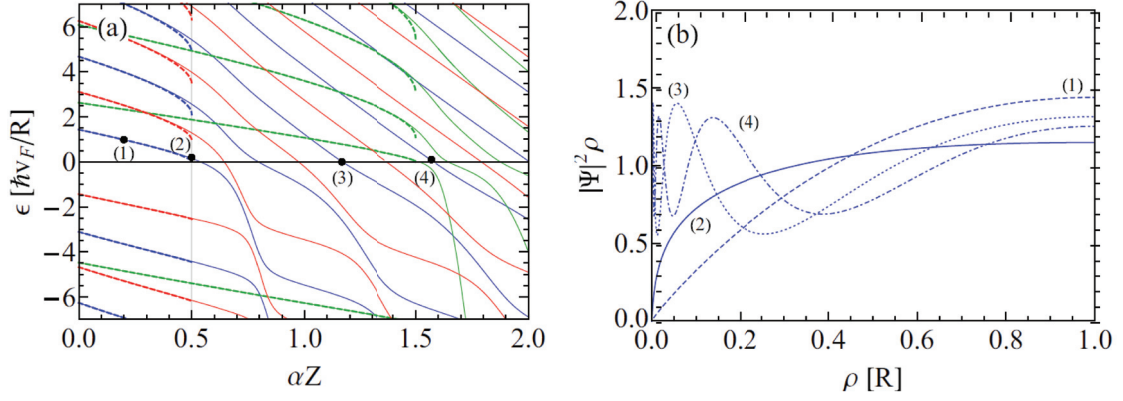


Figure 4.4. (a) Energy spectrum for a dot with a Coulomb impurity. The dashed curves are for a point impurity and the solid ones for a finite size impurity of radius equal to the lattice parameter.(b) Probability density vs ρ for the points labeled by (1) to (4) in (a).(Source: Van Pottelberge et al. (2017))

When we compared our results with the analytic calculations for a circular quantum dot with infinite-mass boundary condition(Berry and Mondragon (1987)) and under the effect of the same Coulomb potential(Fig. 4.4), we see that both results are similar(Van Pottelberge et al. (2017)). The crucial point of that comparison is the working spaces. In our examination we made our Tight-Binding calculations in the real space, the analytical calculations made in the momentum space due to effective-mass approximation. Taking this into account, one can be fascinated due to those similarities.

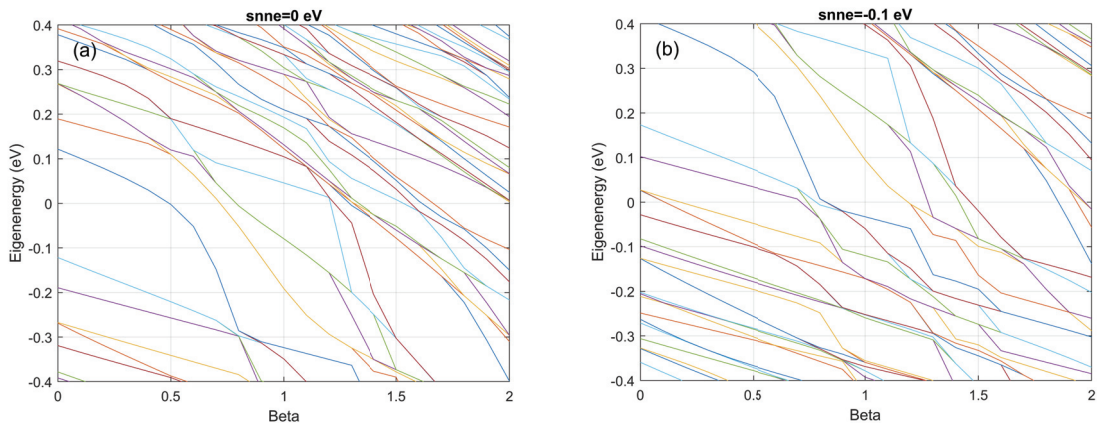


Figure 4.5. (a) TB eigenenergies vs beta for armchair edged hexagonal GQD(5514 Atoms) with $snne=0$ eV and (b) $snne=-0.1$ eV.

Then we make the same TB calculations for a smaller system(5514 Atoms). At this point, our choice of the smaller system is to reduce the time consumption. Because further calculations will include electron-electron interactions and this will take much higher time. So, we will show that the same behaviour still can be observed in this smaller system.

Here, we include the second nearest neighbour energy as -0.1 eV, we clearly see that the energy levels shift about 0.3 eV(Fig. 4.5). However, we also see that the beta value still remain same for the collapsing behaviour. This can be explained by symmetry of the system that is arising from both sublattice symmetry and the central place of the Coulomb potential. We will break soon this symmetry by creating vacancies on the GQD and importance of the snne energy will be seen more clear. Those resemblances generate a reliable ground for the further calculations.

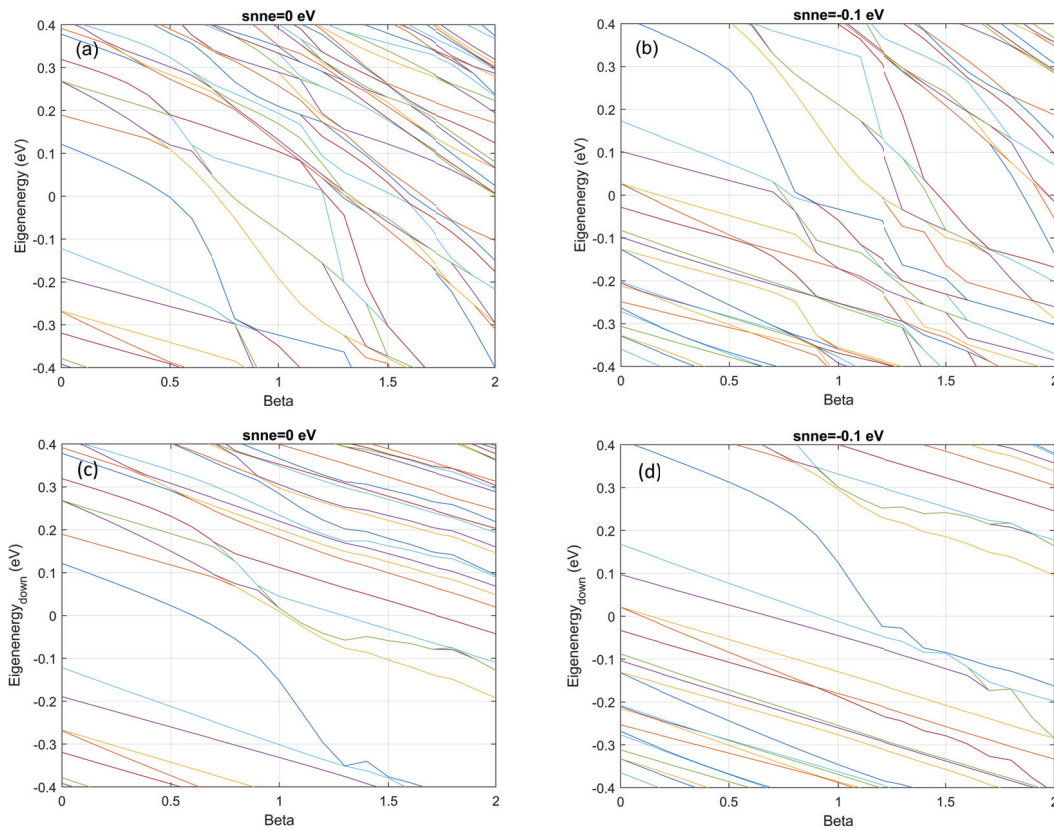


Figure 4.6. (a),(b)Tight Binding and (c),(d) Mean-Field Hubbard results for armchair edged hexagonal GQD(5514 Atoms) with $snne=0$ eV and $snne=-0.1$.

In order to include spins and take a further step to examine the magnetization and correlation effects, we need to electrons' spin characteristics and the electron-electron

interaction into account. In order to introduce that properties, we calculated eigenenergies of the same system by MFH method. Here, we see that starting point of collapsing behaviour shifts to $\beta=0.6$. We are relating that shift is to screening effect(Kotov et al. (2012)). We observe that shift for both $s_{nne}=0$ eV and $s_{nne}=-0.1$ eV cases(Fig. 4.6). Here we only show down spin matrix eigenenergy values because of those are same for up spin matrix values due to symmetry of the system.

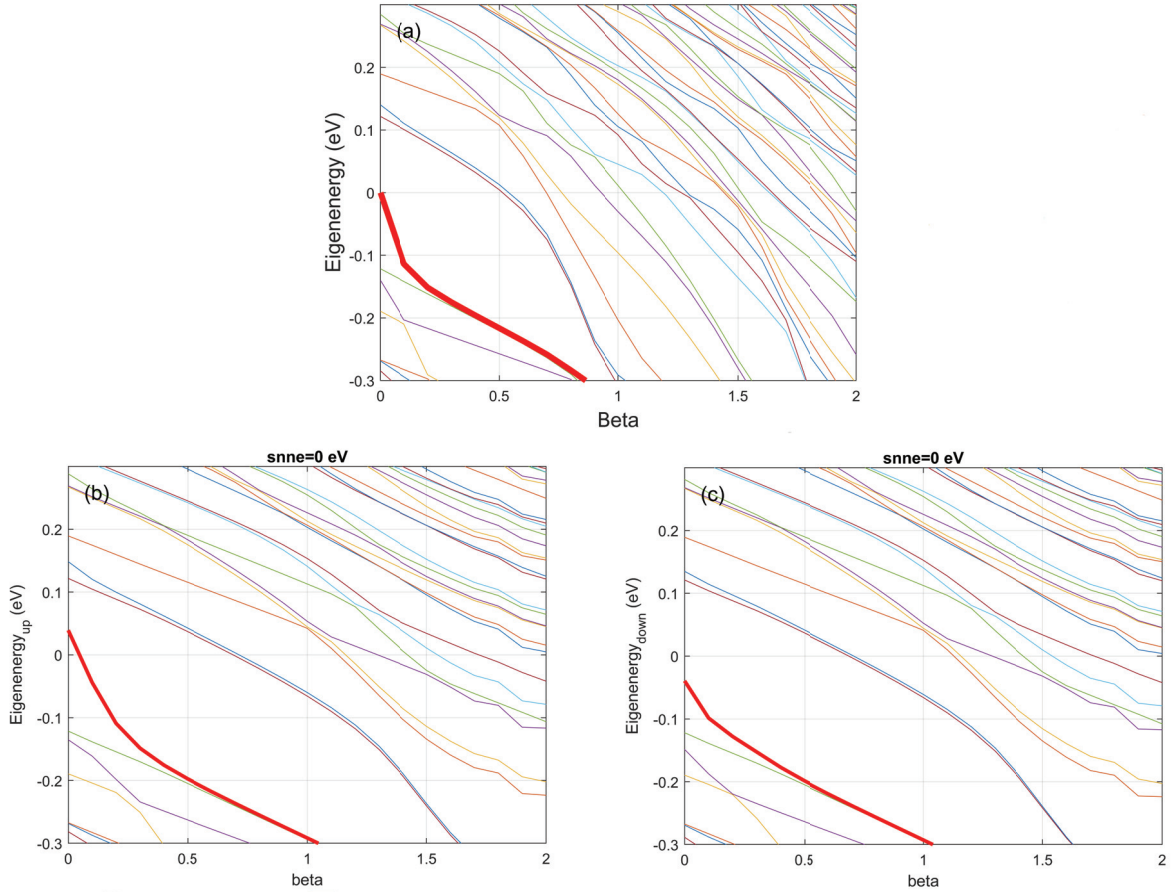


Figure 4.7. (a)Tight Binding results for hexagonal shaped GQD with armchair edge(5513 Atoms), $s_{nne}=0$ eV. Mean-Field Hubbard results (b) up electron and (c) down electron eigenenergies for the same configuration. Red lines stand for the vacancy states.

Tunable artificial atoms at a supercritically charged vacancy in graphene has been observed(Mao et al. (2016)). Considering this, we started with taking out an atom from the dot. While doing that, we chose one of the closest atoms to the center of the dot that we considered as it has an electron with up spin state. Here we see the vacancy state at 0.25 eV at $\beta=0$ for $s_{nne}=-0.1$ eV due to TB result(Fig. 4.7,(a). When we calculated

eigenenergies of same system by MFH method, we observe that the vacancy state shifts above for up spin energies and below for down spin energies with respect to TB result. So, we see that, for the up spin electrons, the band gap is lesser than respect to the band gap for the down spin electrons. Also, with respect to clean dot examination have been made before, the beta value where the collapsing behaviour starts at, shifted from 0.6 to around 0.7(Fig. 4.7 (b),(c)).

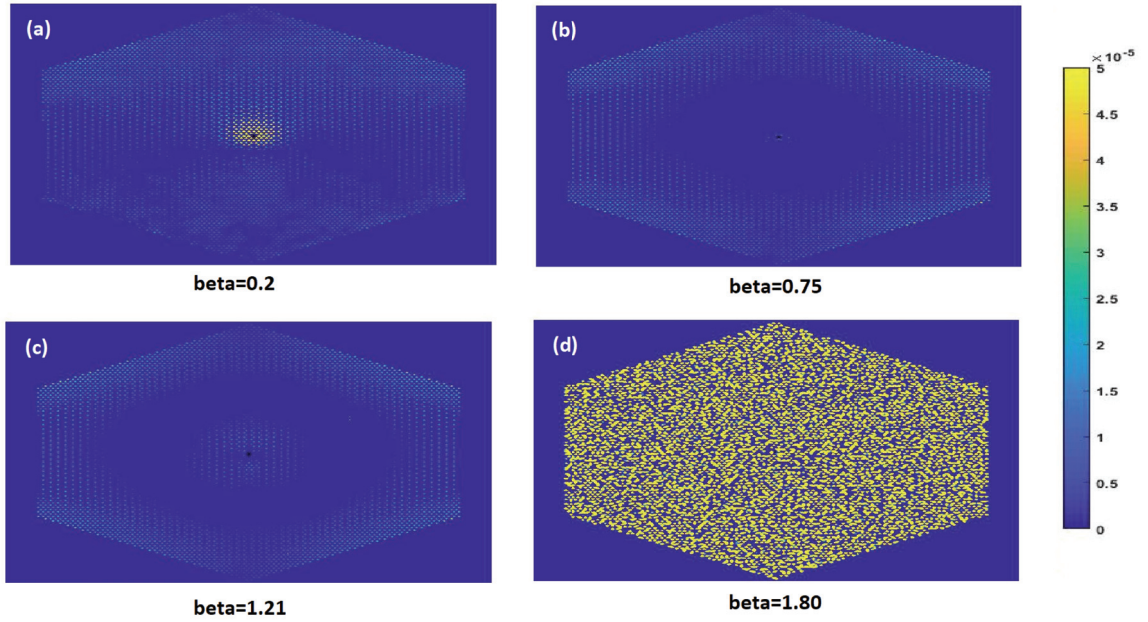


Figure 4.8. Spin densities for the single vacancy configuration with (a) $\beta=0.20$, (b) $\beta=0.75$, (c) $\beta=1.21$, (d) $\beta=1.80$.

On the Other hand, absence of d and f shell electrons is makes an magnetic coupling hard to observe. In graphene substances the source of magnetism are localized electronic states. This localized states can be based on edge types or disorders. Here we see in Fig. (4.8) how spin densities changing with beta for the same single vacancy system. While beta is increasing we are losing localized spins. Because, at the beginning electrons with a particular sign localises around the vacancy. In our single vacancy case, down spins localises around the vacancy because of the removed carbon atom considered as it has an up spin characteristic. While we are increasing the Coulomb potential, at some point, even the opposite signed spins cannot resist to the attraction of the potential and those pulled electrons spoils the local magnetisation.

4.2. Magnetic Correlations Between Defects

To observe correlation and magnetic behaviour due to distance between vacancies, we increased number of vacancies to two. In 1989, E. H. Lieb proved two theorems about ground state magnetism for bipartite lattices, depending on Hubbard model. In both theorems uniqueness of the ground state is also proved. In his work he showed that ground state magnetic moment of a bipartite lattice is equal to half of the subtraction of the number of each lattice sites(Lieb (1989)). In a mathematical description we can show the theorem as,

$$S = \frac{|N_A - N_B|}{2} \quad (4.2)$$

Here, N_A and N_B is number of A and B sublattices respectively.

So, we can use this descriptions as a tool to investigate the magnetic behaviour of our substance, due to its biparticity.

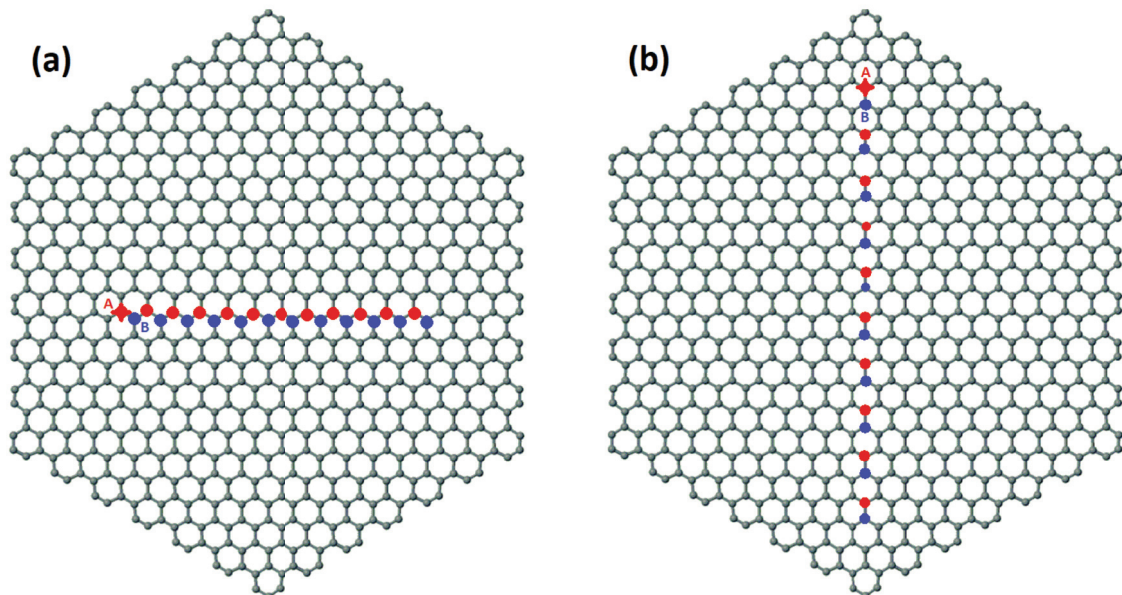


Figure 4.9. Two toy models to show how the vacancies moving along in (a) zigzag and (b) armchair direction. The A site that pointed with the star sign indicates the fixed vacancy. The other vacancy moves on the other points.

First, we tested if the Lieb's theorem is valid for the double vacancy configuration and also the magnetic correlations between the induced spins around the vacancies for different distances between two vacancies and for different second nearest neighbour energies. While we are doing that, we take out an atom from A sublattice at five atom distance from the center of the dot. Here we assume that A sublattice sites have electrons with up spin in ground state and B sublattice sites have electrons with down spin. In every configuration, we hold still this vacancy and changed the position of the other vacancy along the zigzag direction and armchair direction. We take the longest distance between the vacancies as ten atoms in zigzag direction.

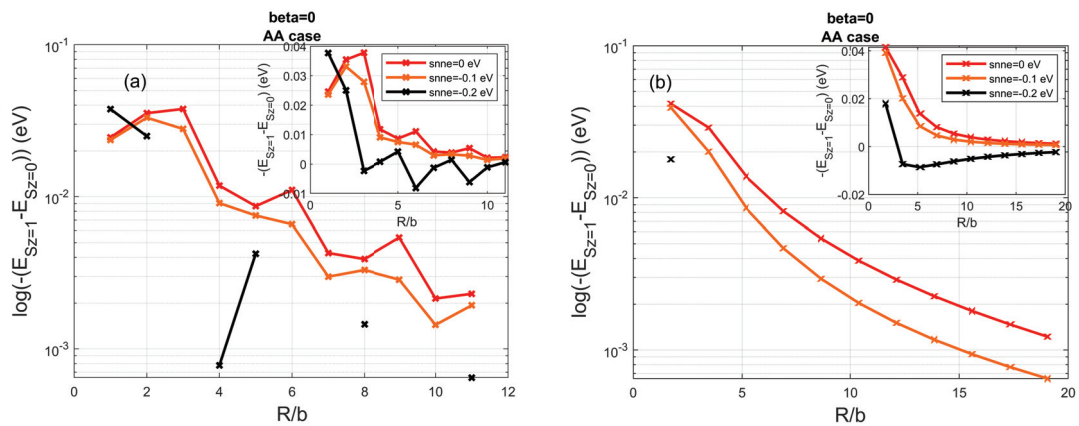


Figure 4.10. Ground state energy difference $-(E_{S_z=1} - E_{S_z=0})$ in logarithmic scale (inset: real) for AA case on (a) zigzag and (b) armchair direction calculated by using MFH for hexagonal GQD with armchair edge with double vacancy(5512 Atoms). The red lines stands for $snne=0$ eV, the orange ones for $snne=-0.1$ and the black ones for $snne=-0.2$ eV.

In the first case, we take out two atoms from two A sublattice sites which represents magnetic moment $S_z = 1$. And also we demonstrated a possible excited state for the same configuration which is made by taking out an atom from an A sublattice site, considering it has an electron with up spin and also taking out an atom from an A sublattice site but assuming it is an electron which has down spin. This system has magnetic moment $S_z = 0$. From now on, we will call both cases as "AA case" and imply the difference by mentioning the magnetic moments.

Energy difference between two configurations, say $E_{S_z=1} - E_{S_z=0}$, gives the energy needed to flip one spin, also this quantity is proportional to magnetic susceptibility and the interaction strength J due to RKKY method(M. Deaven et al. (1991)Ka-

suya (1956)). RKKY method concerns about the indirect interaction between the magnetic impurities which are using host electrons in order to interact (Ruderman and Kittel (1954), Power and Ferreira (2013)). Using this relation we observed the similarities between the correlation behaviour in magnetic impurity modelling and the vacancy type defect modelling along zigzag and armchair direction (Black-Schaffer (2010)).

Because of the expected ground state belongs to $S_z = 1$ configuration due to Lieb's theorem, that difference must be negative. At this point we calculated the energy difference both zigzag and armchair directions and plotted those values respect to R/b . Here b is the next-nearest neighbour distance, which is equals to 2.46 \AA . Also we calculated $E_{S_z=1} - E_{S_z=0}$ difference for different snne values 0 eV, -0.1 eV, and -0.2 eV. We observed that, Lieb's theorem doesn't hold for snne=-0.2 eV (Fig. 4.10) on both zigzag and armchair directions. Here we used $-(E_{S_z=1} - E_{S_z=0})$ instead of the $E_{S_z=1} - E_{S_z=0}$ in order to show the logarithmic scale in negative values.

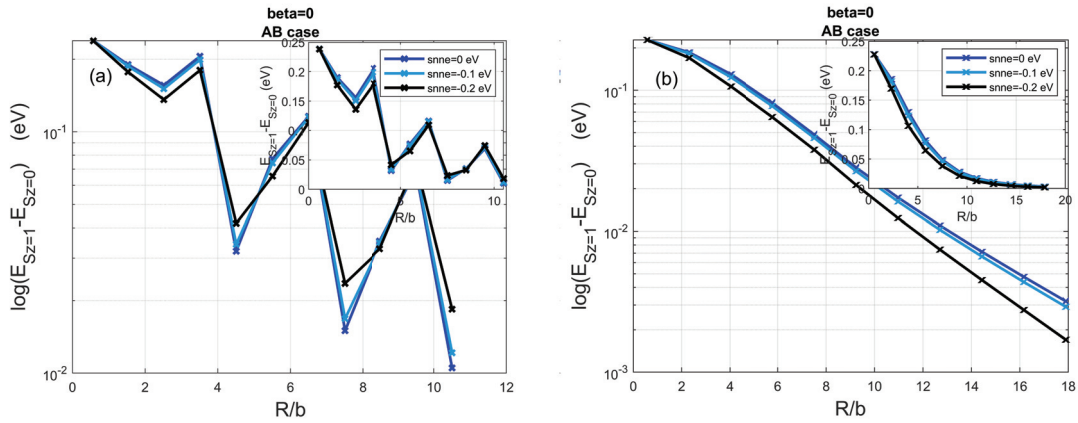


Figure 4.11. Ground state energy difference $E_{S_z=1} - E_{S_z=0}$ in logarithmic scale (inset: real) for AB case on (a) zigzag and (b) armchair direction calculated by using MFH for hexagonal GQD with armchair edge with double vacancy (5512 Atoms). The dark blue lines stands for snne=0 eV, the light blue ones for snne=-0.1 and the black ones for snne=-0.2 eV.

Then we made similar things for the second vacancy configuration. We take out an atom from an A sublattice site and one atom from a B sublattice site which represents magnetic moment $S_z = 0$. Also again, we demonstrated a possible excited state for the same configuration which is made by taking out an atom from an A sublattice site, considering it has an electron with up spin and also taking out an atom from an B sublattice site but assuming it has an electron which has also up spin. This system has magnetic

moment $S_z = 1$. From now on, we will call both cases as "AB case" and imply the difference by mentioning the magnetic moments. In this part, the ground state must be the $S_z = 0$ configuration. So, $E_{S_z=1} - E_{S_z=0}$ difference must be positive for this configuration. In this case, we observe that even for $\text{snne}=-0.2$ eV, Lieb's theorem holds on both zigzag and armchair directions(Fig. 4.11).

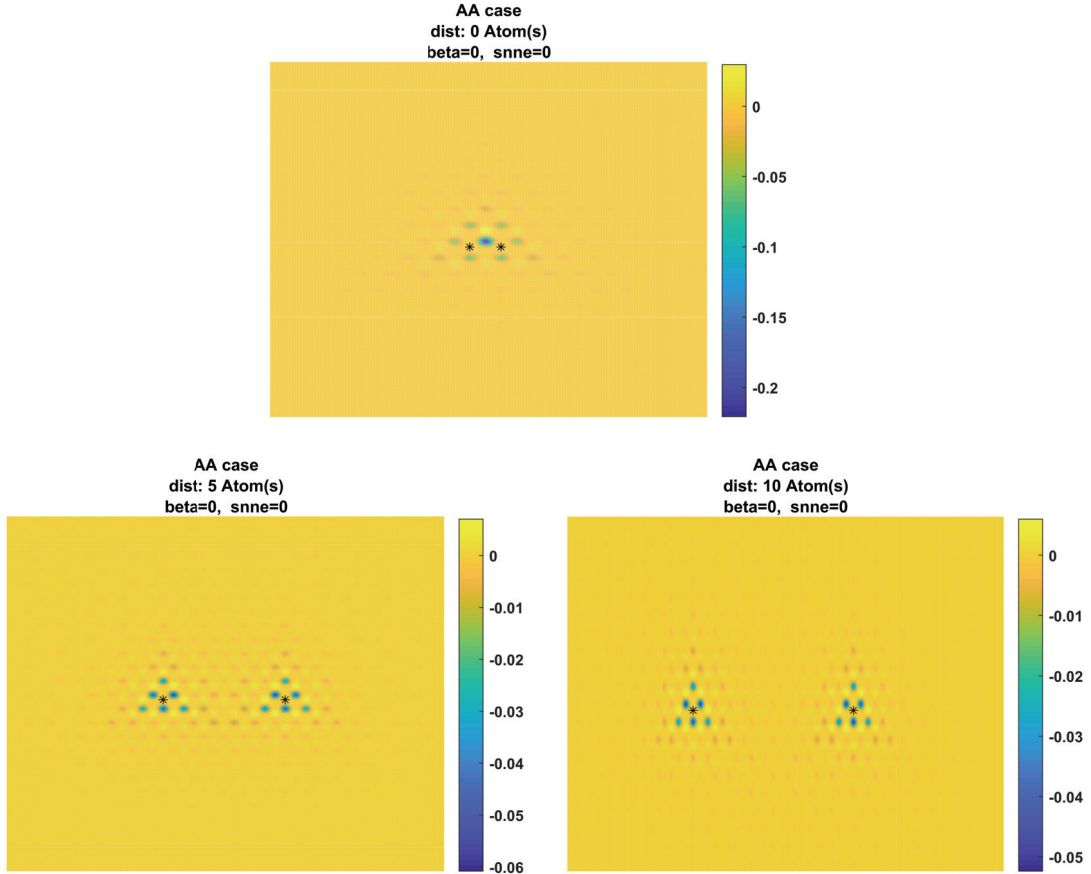


Figure 4.12. Spin densities for the two vacancy AA configuration for distance(a) 0 atom, (b) 5 atoms, and(c) 10 atoms.

Here we see in Fig. 4.12 spin densities for AA case for $\beta=0$ and $\text{snne}=0$ eV. Due to absence of up spins, a localised magnetisation includes around the vacancy by down spin electrons. Closer the distance between the vacancies, correlation effects become higher.

Since we decided proper snne values, we can include the effect of Coulomb potential at the vacancy centers and examine how the magnetization changes while the β value changes. In the Fig. 4.13, $E_{S_z=1} - E_{S_z=0}$ values on top are calculated along the zigzag direction, and the bottom ones are along the armchair direction. Here we see anti-ferromagnetic phase transition for AA case when we take $\beta=0.1$. Moreover, when we

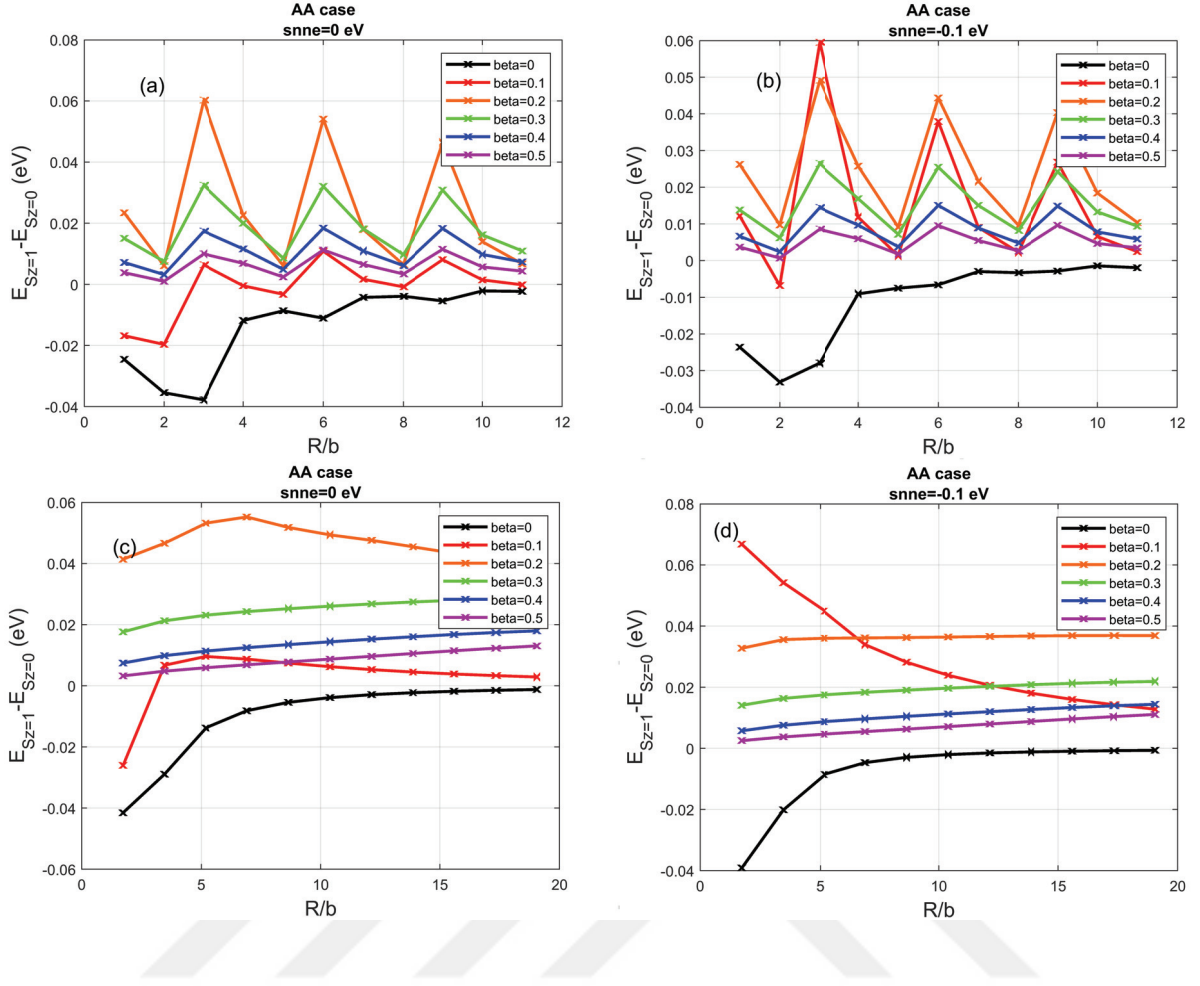


Figure 4.13. Ground state energy difference $E_{S_z=1} - E_{S_z=0}$ for AA case on zigzag direction for (a) $snne=0$ eV, (b) $snne=-0.1$ eV and armchair direction for (c) $snne=0$ eV, (d) $snne=-0.1$ eV calculated by using MFH for hexagonal GQD with armchair edge with double vacancy(5512 Atoms).

compare on both directions(zigzag, armchair), we see at $\beta=0.1$, graphs show dramatic differences depending on inclusion of the second nearest neighbour energy($snne=-0.1$ eV). Orders of energy difference $E_{S_z=1} - E_{S_z=0}$ are close for the other β values. Also, if we keep increasing the β value, $E_{S_z=1} - E_{S_z=0}$ goes to zero, gradually.

We see in Fig. 4.14, opposite type phase transition is not valid for AB case. Again, values on top are calculated along the zigzag direction, and the bottom ones are along the armchair direction. In a simple look, we can say that the interaction strength decreases and magnetism dies with increasing β for both AA and AB case. To explain the phase transition in AA case, we investigate the possible relation between energy levels and the distance between the vacancies while β value varies.

In the Fig. (4.15), we draw few necessary states that can effect the phase transition.

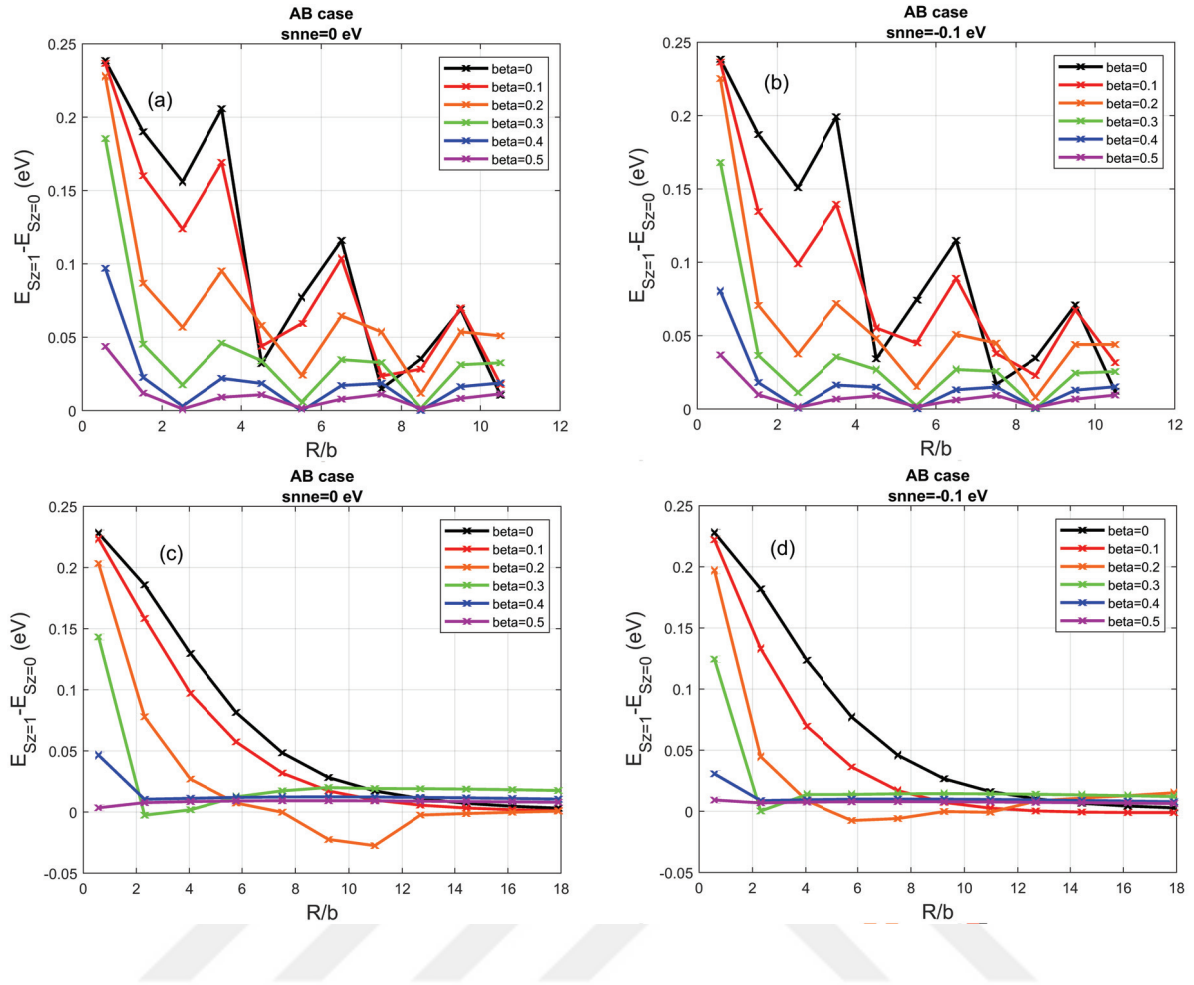


Figure 4.14. Ground state energy difference $E_{S_z=1} - E_{S_z=0}$ for AB case on zigzag direction for (a) $snne=0$ eV, (b) $snne=-0.1$ eV and armchair direction for (c) $snne=0$ eV, (d) $snne=-0.1$ eV calculated by using MFH for hexagonal GQD with armchair edge with double vacancy(5512 Atoms).

Every different colour describes a state and every single line stands for a different distance value between the vacancies. Here, we can see that energy difference between the vacancy states are changing more dramatically than the other above states. How this energy gap between the vacancy states change, gives the information about the most favourable spin orientation.

We know that while $\beta=0$ (also the ground state) expected behaviour of magnetism is ferromagnetic for AA case. While β changes, the system becomes excited and spins can flip in order to be in a favourable low energy state. When we take out two up spin electrons from the A sites, we left with two down spins more. Those down spins will be in the different energy levels due to Pauli exclusion principle. But, if the energy difference between those levels are high, the electron on the above energy level would

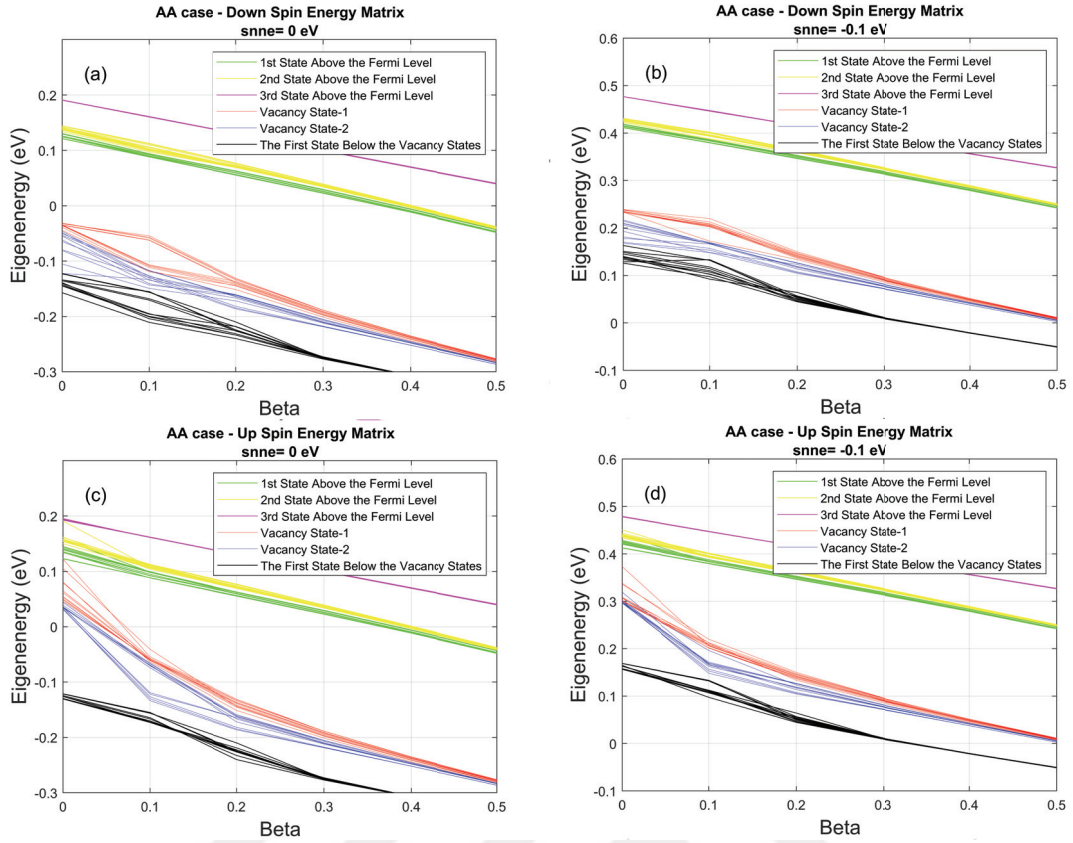


Figure 4.15. The first and second vacancy states and the the first three states above the fermi level on zigzag direction

prefer to flip its sign to lower the systems energy. That will cause the anti-ferromagnetic ordering. So, in AA case if the energy gap between the vacancy states is high, electrons expected to be in an anti-ferromagnetic alignment.

Fig. 4.16 is to show how these difference changes between the states respect to beta and the distance between the vacancies on zigzag direction. Here, we cannot detect an exact correspondence between $E_{S_z=1} - E_{S_z=0}$ difference and eigenenergy difference between the vacancy states for both AA and AB case. So, the physical explanation of phase transition that we observed in AA case remained unknown. To examine how the magnetization of the GQD with atomic collapse, we can look at Fig. (4.15) again. To determine the beta value that atomic collapse starts, we use the graph with snne=0 eV(4.15 (a), (c)). Then we see that atomic collapse first occurs around beta=0.35. When we check that value on the Fig. (4.16 (a),(c)), we detect no distinc behaviour then the other beta values. Also again, we detect no relation between the atomic collapse and the magnetic phase transition.

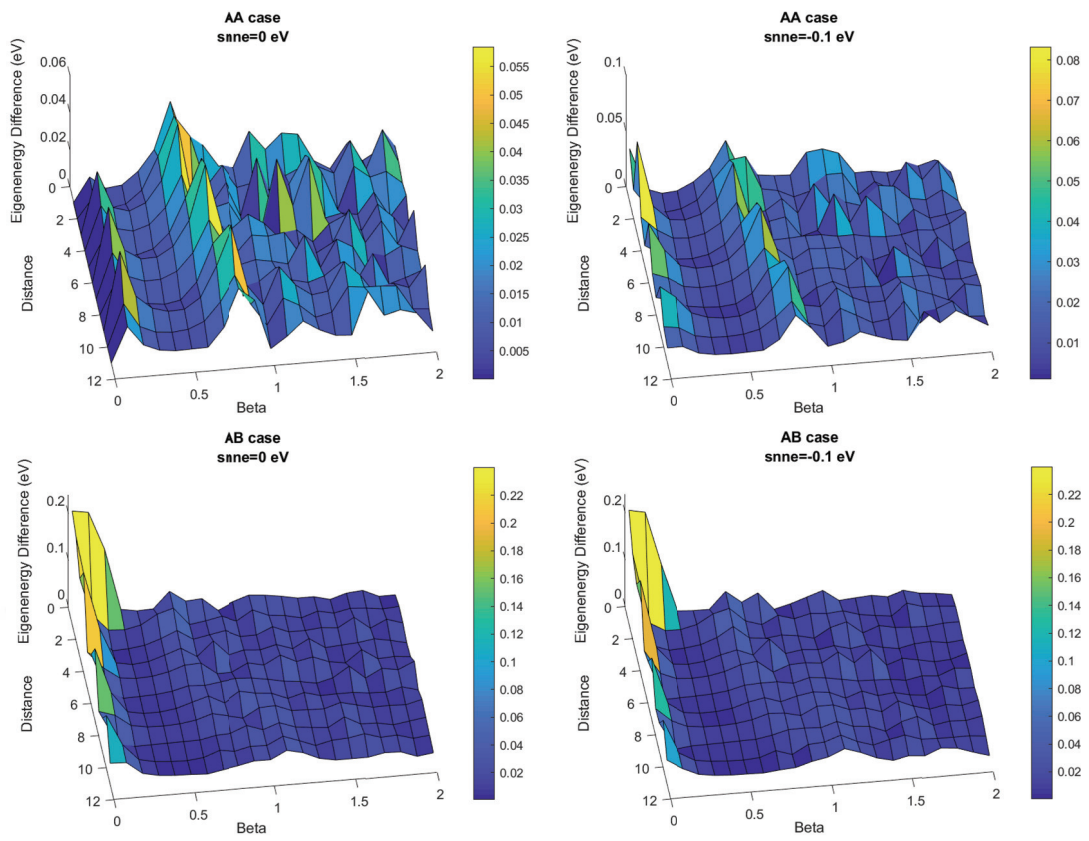


Figure 4.16. AA case on zigzag direction. TB eigenenergy difference between the vacancy states for AA case with (a) $s_{sne}=0$ eV, (b) $s_{sne}=-0.1$ eV, and AB case with (c) $s_{sne}=0$ eV, (d) down spin energy matrix with $s_{sne}=-0.1$ eV

CHAPTER 5

CONCLUSION

In this thesis various defect types examined on hexagonal shaped GQD with armchair edge in different context. Atomic collapse behaviour is examined on hexagonal GQD with armchair edge. When the Coulomb potential applied to the center of the dot, we see tight-binding calculations agrees with analytic calculations while inspecting atomic collapse behaviour. As applied Coulomb potential increases, probability of finding an electron around the potential center, increases. When mean-field Hubbard calculations are examined for the same central potential problem; we observe, beta values needed to observe atomic collapse behaviour are found higher respect to tight-binding calculations due to screening. For the dots with double vacancy, increasing Coulomb potential and increasing distance between the vacancies, reduces correlations of electrons around the vacancies. Related calculations for interaction strength show similar decreasing fluctuations along zigzag direction and smooth decreasing behaviour along armchair direction. Also changing potential leads to ferromagnetic-anti-ferromagnetic phase transition, independent from the atomic collapse behaviour(for AA case). Also we observed that there is no direct link between the magnetic transition and the energy difference of the vacancy states.

At this point further investigations will be illuminating. One option is applying the Coulomb potential directly onto atoms without taking any atom out from the dot. While doing that the Coulomb potential must be applied onto the same positions with the positions of the vacancies investigated in this thesis. Examining the differences between two investigations probably will give a perceivable explanation about how our method and RKKY interaction related, by means of magnetization and couplings, in this system. Also changing vacancy positions close to edges would change the beta value that magnetic phase transition were happened.

REFERENCES

- Altintas, A., K. Cakmak, and A. Guclu (2017, 01). Effects of long-range disorder and electronic interactions on the optical properties of graphene quantum dots. *Physical review. B, Condensed matter* 95.
- Anderson, C. D. (1933, Mar). The positive electron. *Phys. Rev.* 43, 491–494.
- Ando, T. and T. Nakanishi (1998). Impurity scattering in carbon nanotubes absence of back scattering. *Journal of the Physical Society of Japan* 67(5), 1704–1713.
- Ando, T., Y. Zheng, and H. Suzuura (2002). Dynamical conductivity and zero-mode anomaly in honeycomb lattices. *Journal of the Physical Society of Japan* 71(5), 1318–1324.
- Berger, C., Z. Song, T. Li, X. Li, A. Y. Ogbazghi, R. Feng, Z. Dai, A. N. Marchenkov, E. H. Conrad, P. N. First, and W. A. de Heer (2004). Ultrathin epitaxial graphite 2d electron gas properties and a route toward graphene-based nanoelectronics. *The Journal of Physical Chemistry B* 108(52), 19912–19916.
- Berry, M. V. and R. J. Mondragon (1987). Neutrino billiards: time-reversal symmetry-breaking without magnetic fields. *Proceedings of the Royal Society of London. A. Mathematical and Physical Sciences* 412(1842), 53–74.
- Black-Schaffer, A. M. (2010, May). Rkky coupling in graphene. *Phys. Rev. B* 81, 205416.
- Boukhvalov, D. W. and M. I. Katsnelson (2008). Modeling of graphite oxide. *Journal of the American Chemical Society* 130(32), 10697–10701.
- Brdoie, B. C. (1859). On the atomic weight of graphite. *Philosophical Transactions of the Royal Society of London.*
- Castro Neto, A. H., F. Guinea, N. M. R. Peres, K. S. Novoselov, and A. K. Geim (2009, Jan). The electronic properties of graphene. *Rev. Mod. Phys.* 81, 109–162.

- Collins, P. G. (2009). Defects and disorder in carbon nanotubes.
- Cowan, T., H. Backe, M. Begemann, K. Bethge, H. Bokemeyer, H. Folger, J. S. Greenberg, H. Grein, A. Gruppe, Y. Kido, M. Kluver, D. Schwalm, J. Schweppe, K. E. Stiebing, N. Trautmann, and P. Vincent (1985, Apr). Anomalous positron peaks from supercritical collision systems. *Phys. Rev. Lett.* 54, 1761–1764.
- Darwin, C. G. (1928). The wave equations of the electron. *Proceedings of the Royal Society of London. Series A, Containing Papers of a Mathematical and Physical Character* 118(780), 654–680.
- Dirac, P. A. M. and R. H. Fowler (1928a). The quantum theory of the electron. *Proceedings of the Royal Society of London. Series A, Containing Papers of a Mathematical and Physical Character* 117(778), 610–624.
- Dirac, P. A. M. and R. H. Fowler (1928b). The quantum theory of the electron. part ii. *Proceedings of the Royal Society of London. Series A, Containing Papers of a Mathematical and Physical Character* 118(779), 351–361.
- Dirac, P. A. M. and R. H. Fowler (1930). A theory of electrons and protons. *Proceedings of the Royal Society of London. Series A, Containing Papers of a Mathematical and Physical Character* 126(801), 360–365.
- Eder, R. (2017). Introduction to the hubbard model. In *The Physics of Correlated Insulators, Metals, and Superconductors Lecture Notes of the Autumn School on Correlated Electrons 2017*. Ed. E. Pavarini, Volume 7 of *Schriften des Forschungszentrums Julich Reihe Modeling and Simulation*, pp. 145–173. Forschungszentrum Julich, Julich.
- Gordon, W. (1926). Der comptoneffekt nach der schrodingerschen theorie. *Zeitschrift fur Physik* 40(1), 117–133.
- Guclu, A.D., P. P. K. M. H. P. (2014). *Graphene Quantum Dots*. Springer.
- Hummers, W. S. and R. E. Offeman (1958). Preparation of graphitic oxide. *Journal of the American Chemical Society* 80(6), 1339–1339.

- Juang, Z.-Y., C.-Y. Wu, A.-Y. Lu, C.-Y. Su, K.-C. Leou, F.-R. Chen, and C.-H. Tsai (2010). Graphene synthesis by chemical vapor deposition and transfer by a roll-to-roll process. *Carbon* 48(11), 3169 – 3174.
- Kasuya, T. (1956, 07). A Theory of Metallic Ferro- and Antiferromagnetism on Zener's Model. *Progress of Theoretical Physics* 16(1), 45–57.
- Kaxiras, E. and K. C. Pandey (1988, Dec). Energetics of defects and diffusion mechanisms in graphite. *Phys. Rev. Lett.* 61, 2693–2696.
- Klein, O. (1927, Oct). Elektrodynamik und wellenmechanik vom standpunkt des korrespondenzprinzips. *Zeitschrift fur Physik A Hadrons and nuclei* 41(6), 407–442.
- Kotov, V. N., B. Uchoa, V. M. Pereira, F. Guinea, and A. H. Castro Neto (2012, Jul). Electron-electron interactions in graphene: Current status and perspectives. *Rev. Mod. Phys.* 84, 1067–1125.
- Li, L., G. Wu, G. Yang, J. Peng, J. Zhao, and J.-J. Zhu (2013). Focusing on luminescent graphene quantum dots: current status and future perspectives. *Nanoscale* 5, 4015–4039.
- Liang, X. (2014). Chapter 19 - transition from tubes to sheets-a comparison of the properties and applications of carbon nanotubes and graphene. In M. J. Schulz, V. N. Shanov, and Z. Yin (Eds.), *Nanotube Superfiber Materials*, pp. 519 – 568. William Andrew Publishing.
- Lieb, E. H. (1989, Mar). Two theorems on the hubbard model. *Phys. Rev. Lett.* 62, 1201–1204.
- Liu, K., P. Yan, J. Li, C. He, T. Ouyang, C. Zhang, C. Tang, and J. Zhong (2017, 12). Effect of hydrogen passivation on the decoupling of graphene on sic(0001) substrate: First-principles calculations. *Scientific Reports* 7.
- M. Deaven, D., D. S. Rokhsar, and M. Johnson (1991, 10). Simple theory of exchange coupling in transition-metal magnetic multilayers. *Physical review. B, Condensed matter* 44, 5977–5980.
- Mao, J., Y. Jiang, D. Moldovan, G. Li, K. Watanabe, T. Taniguchi, M. R. Masir, F. M.

Peeters, and E. Y. Andrei (2016, Feb). Realization of a tunable artificial atom at a supercritically charged vacancy in graphene. *Nature Physics* 12, 545 EP –.

Moldovan, D. and F. M. Peeters (2016). Atomic collapse in graphene. In J. Bonča and S. Kruchinin (Eds.), *Nanomaterials for Security*, Dordrecht, pp. 3–17. Springer Netherlands.

Neto, A. C., F. Guinea, and N. M. Peres (2006, nov). Drawing conclusions from graphene. *Physics World* 19(11), 33–37.

Nikolai A. Poklonski, Eugene F. Kislyakov, S. A. V. O. N. B. S. V. R. (2012). Electronic band structure and magnetic states of zigzag graphene nanoribbons: quantum chemical calculations. *Journal of Nanophotonics* 6(1), 1 – 9 – 9.

Novoselov, K. S., V. I. Fal'ko, L. Colombo, P. R. Gellert, M. G. Schwab, and K. Kim (2012). A roadmap for graphene. *Nature* 490, 192–200.

Novoselov, K. S., A. K. Geim, S. V. Morozov, D. Jiang, Y. Zhang, S. V. Dubonos, I. V. Grigorieva, and A. A. Firsov (2004). Electric field effect in atomically thin carbon films. *Science* 306(5696), 666–669.

Pieper, W. and W. Greiner (1969, Aug). Interior electron shells in superheavy nuclei. *Zeitschrift fur Physik A Hadrons and nuclei* 218(4), 327–340.

Pomeranchuk, I. and Y. Smorodinsky (1945). On the energy levels of systmes with $z > 137$. *J. Phys. USSR* (9), 97.

Power, S. and M. Ferreira (2013, 01). Indirect exchange and ruderman-kittel-kasuya-yosida (rkky) interactions in magnetically-doped graphene. *Crystals* 3.

Reina, A., X. Jia, J. Ho, D. Nezich, H. Son, V. Bulovic, M. S. Dresselhaus, and J. Kong (2009). Large area, few-layer graphene films on arbitrary substrates by chemical vapor deposition. *Nano Letters* 9(1), 30–35.

Ruderman, M. A. and C. Kittel (1954, Oct). Indirect exchange coupling of nuclear magnetic moments by conduction electrons. *Phys. Rev.* 96, 99–102.

Schrodinger, E. (1926). Quantisierung als eigenwertproblem. *Annalen der Physik* 384(4), 361–376.

Schweppe, J., A. Gruppe, K. Bethge, H. Bokemeyer, T. Cowan, H. Folger, J. S. Greenberg, H. Grein, S. Ito, R. Schule, D. Schwalm, K. E. Stiebing, N. Trautmann, P. Vincent, and M. Waldschmidt (1983, Dec). Observation of a peak structure in positron spectra from u+cm collisions. *Phys. Rev. Lett.* 51, 2261–2264.

Sheng, W.-d., M. Korkusinski, A. D. Güçlü, M. Zielinski, P. Potasz, E. S. Kadantsev, O. Voznyy, and P. Hawrylak (2012, Jun). Electronic and optical properties of semiconductor and graphene quantum dots. *Frontiers of Physics* 7(3), 328–352.

Shytov, A., M. Katsnelson, and L. S Levitov (2008, 01). Vacuum polarization and screening of supercritical impurities in graphene. *Physical review letters* 99, 236–801.

Shytov, A. V., M. I. Katsnelson, and L. S. Levitov (2007). Atomic collapse and quasi-rydberg states in graphene. *Phys. Rev. Lett.* 99, 246802.

Soff, Gerhard, B. M. and J. Rafelski. Precise values for critical fields in quantum electrodynamics. *Zeitschrift für Naturforschung* 29a, 1267–1275.

Soff, G., U. Muller, T. de Reus, J. Reinhardt, B. Muller, and W. Greiner (1985). Atomic excitations in supercritical fields of giant nuclear systems. *Nuclear Instruments and Methods in Physics Research Section B: Beam Interactions with Materials and Atoms* 10-11, 214 – 218.

Sommerfeld, A. (1919). *Atombau und Spektrallinien*. Vieweg, Braunschweig.

Stankovich, S., D. A. Dikin, R. D. Piner, K. A. Kohlhaas, A. Kleinhammes, Y. Jia, Y. Wu, S. T. Nguyen, and R. S. Ruoff (2007). Synthesis of graphene-based nanosheets via chemical reduction of exfoliated graphite oxide. *Carbon* 45(7), 1558 – 1565.

Staudenmaier, L. (1898). Verfahren zur darstellung der graphitsaure. *Berichte der deutschen chemischen Gesellschaft* 31(2), 1481–1487.

Tian, P., L. Tang, K. Teng, and S. Lau (2018). Graphene quantum dots from chemistry to applications. *Materials Today Chemistry* 10, 221 – 258.

Vafek, O. and A. Vishwanath (2014). Dirac fermions in solids from high-*t_c* cuprates and graphene to topological insulators and weyl semimetals. *Annual Review of Condensed Matter Physics* 5(1), 83–112.

Van Pottelberge, R., M. Zarenia, P. Vasilopoulos, and F. M. Peeters (2017, 06). Graphene quantum dot with a coulomb impurity: Subcritical and supercritical regime. *Physical Review B* 95.

Wallace, P. R. (1947, May). The band theory of graphite. *Phys. Rev.* 71, 622–634.

Wang, Y., D. Wong, A. Shytov, V. W Brar, S. Choi, Q. Wu, H.-Z. Tsai, W. Regan, A. Zettl, R. Kawakami, S. G Louie, L. S Levitov, and M. F Crommie (2013, 03). Observing atomic collapse resonances in artificial nuclei on graphene. *Science (New York, N.Y.)* 340.

Wang, Y., D. Wong, A. V. Shytov, V. W. Brar, S. Choi, Q. Wu, H.-Z. Tsai, W. Regan, A. Zettl, R. K. Kawakami, S. G. Louie, L. S. Levitov, and M. F. Crommie (2013). Observing atomic collapse resonances in artificial nuclei on graphene. *Science* 340(6133), 734–737.

Werner, F. G. and J. A. Wheeler (1958, Jan). Superheavy nuclei. *Phys. Rev.* 109, 126–144.